Monotonic and cyclic undrained behaviour and liquefaction resistance of pumiceous, non-plastic sandy silt

Jordanka Chaneva*[1], Max O. Kluger[2], Vicki G. Moon[3], David J. Lowe[4], Rolando P. Orense[5]

*Corresponding author

[1]School of Science/Te Aka Mātuatua, University of Waikato, Hamilton, New Zealand, jc409@students.waikato.ac.nz

[2]School of Science/Te Aka Mātuatua, University of Waikato, Hamilton, New Zealand, max.kluger@waikato.ac.nz; https://orcid.org/0000-0001-9130-8948

[3]School of Science/Te Aka Mātuatua, University of Waikato, Hamilton, New Zealand, vicki.moon@waikato.ac.nz

[4]School of Science/Te Aka Mātuatua, University of Waikato, Hamilton, New Zealand, david.lowe@waikato.ac.nz; https://orcid.org/0000-0002-2547-6019

[5]Department of Civil and Environmental Engineering, University of Auckland, New Zealand, r.orense@auckland.ac.nz

This article is the final accepted version of a paper published subsequently in *Soil Dynamics and Earthquake Engineering* vol. 168, article 107825 (2023).

https://doi.org/10.1016/j.soildyn.2023.107825

Abstract

Experimental data related to the mechanical behaviour of crushable pumiceous soils are limited compared with those for hard-grained soils. The main focus of previous studies has been on pumiceous sands, whereas pumiceous silts have not been investigated to date. In this paper, several series of monotonic and cyclic triaxial tests were performed to investigate the undrained behaviour and liquefaction resistance of a natural volcanic-ash derived non-plastic pumiceous silt from northern New Zealand. Particle crushing due to sample reconstitution and triaxial testing was analysed by quantifying the changes in grain-size parameters and pumice contents. The main results can be summarized as follows. (1) The pumiceous silt showed a contractive response, even at medium to high relative densities, leading to high flow liquefaction susceptibility. (2) When subjected to cyclic undrained loading, the silt exhibited similar trends in terms of excess pore water pressure and axial strain accumulation to those established for hard-grained soils as opposed to those for pumiceous sands. (3) The liquefaction resistance of both medium-dense and dense samples was within the lower range compared to published cyclic resistance curves of both hard-grained soils and pumiceous sands. (4) The material did not undergo significant particle crushing after testing. Result (4) was considered to be the main factor that contributed to the fact that, in general, the cyclic undrained behaviour of the pumiceous silt was close to the trends established for those of hard-grained soils.

Keywords: pumice; volcanic soil; silt; liquefaction; undrained triaxial tests; state parameter; lake sediment; tephra

Notation list

A_c	angular coefficient
A_r	aspect ratio
CSL	critical state line
CSR	cyclic stress ratio
D_{50}	median grain size
D_{10}	grain size at 10% passing
D_{90}	grain size at 90% passing
Dr	relative density
$Dr_{,i}$	initial relative density
$Dr_{,c}$	consolidated relative density
e	void ratio
e_c	consolidated void ratio
e_i	initial void ratio
e_{max}	maximum void ratio
e_{min}	minimum void ratio
e_{ss}	void ratio at the steady state line
EPWP	excess pore water pressure
f	loading frequency
FC	fines content
Gs	specific gravity
N_C	number of cycles
N_{CL}	number of cycles to liquefaction
p'	mean effective stress
PC	pumice content
q	deviator stress
r_u	pore pressure ratio
R_c	roundness coefficient
SD	standard deviation
u	pore pressure
σ_c'	effective consolidation pressure
ε_{da}	double amplitude axial strain
ψ	state parameter

1. Introduction

Earthquake-induced liquefaction can be a major natural hazard in tectonically active regions [1,2], hence undrained soil response and liquefaction initiation analyses have been of particular interest in the past six decades. The scientific and engineering community recognizes two main definitions of liquefaction, (1) flow liquefaction, characterized with strain-softening response in undrained loading and it requires in-situ shear stress greater than the undrained shear strength, and (2) cyclic liquefaction, characterized with pore water pressure build up on account of the effective stress reversal to zero. Flow liquefaction can be triggered by both monotonic and cyclic loading. It is also commonly used when defining cyclic liquefaction susceptibility based on the state criteria: in critical soil mechanics, soils susceptible to flow liquefaction are also defined as contractive, thus loose materials that are highly susceptible to cyclic liquefaction as well [3–5].

Since the early works from the 1970s [6–8], most of the research related to soil liquefaction has been focused on hard-grained sands and silts, because the common liquefaction susceptible soils were originally considered to be young (i.e., of Holocene age), non- or low-plastic, normally consolidated, hard-grained sandy soils [9,10]. More recent case studies, however, have confirmed the vulnerability of crushable materials, such as pumiceous volcanic soils, to liquefaction as well [11–15]. Therefore, in the last few decades, pumiceous sands have become a topic of interest for researchers and geotechnical engineers working in tectonically active areas, such as Italy, South America, Japan, and the North Island of New Zealand [16–19]. Pure pumiceous soils consist of volcanically-derived vesicular, lightweight glass-shard particles of grain sizes varying between gravel (lapilli), sand (coarse to medium ash), and fines (fine ash) [20].

For coarse-grained pumiceous soils mainly comprising sand-sized particles, it has been demonstrated that under monotonic undrained loading, the relative density did not have significant effect on the behaviour, as samples in both loose and dense states practically showed similar response [12]. Orense and Pender [12] found that even at large strain level, pumice sands did not reach steady state of deformation, and inferred that the critical soil mechanics may not be applicable to crushable soils.

During cyclic undrained tests, pumiceous sands show different trends in terms of axial strain and excess pore water pressure (EPWP) development [13], when compared with those for hard-grained sands. For example, Asadi et al. [13] found that unlike hard-grained sands, where the development of the EPWP as well as the axial strain increased in a sudden manner in the last loading cycles, pumiceous sands tend to show immediate increase of both the EPWP and the axial strain in the first loading cycles. Moreover, because of the

dilative response of pumiceous sands in the succeeding loading cycles, after the initial cycles, the liquefaction resistance of the pumice sands may be significantly higher than that obtained for hard-grained soils [11,13]. The findings related to the monotonic undrained behaviour of pumice sands [12], as well as the different EPWP development and the higher liquefaction resistance of pumiceous sands compared with that of hard-grained sands [11,13], have all been attributed to the vesicular nature as well as the complex surface texture of the pumiceous particles, which which leads to significant particle crushing during cyclic loading, especially in samples with high relative densities.

Studies on the undrained behaviour and liquefaction resistance of pumiceous sands containing non-plastic fines are even more scarce than studies on pure pumiceous sands [14,21]. In the study by Licata et al. [14], it was found that a pumiceous silty sand mixture with 30% non-plastic fines exhibited a higher liquefaction resistance compared with hard-grained silica sand having the same proportion of fines. They reported negligible particle crushing in their pumiceous material. In contrast, in a more recent study, Hyodo et al. [21] examined a pumiceous silty sand (Shirasu) comprising pumiceous sand with 28% fines and found the pumiceous silty sand to be less resistant to liquefaction than pure Shirasu sand. However, Hyodo et al. did not discuss the level of particle crushing that might have occurred in the Shirasu sand.

Studies focusing on the cyclic undrained behaviour and liquefaction resistance of pumiceous silts (mixtures containing >50% fines) have not been reported to date. Therefore, filling the knowledge gaps for this type of soil materials will assist scientists as well as geotechnical practitioners who are unsure whether they should treat silt-size pumice materials the same as sand-size ones.

This paper is based on a wider testing campaign studying the undrained behaviour and liquefaction resistance of non-plastic pumiceous sandy silt sampled from a silica-rich tephra layer of mid-Holocene age. Tephra deposits are the volcanic-eruption-derived, pyroclastic products of a volcanic eruption of any grain size or composition [22]. The tephra layer, preserved within the sediments of riverine-peat lakes in the Hamilton lowlands, North Island, New Zealand, has been found to show proof of paleoliquefaction [23]. Knowledge about the undrained response of the tephra is crucial in evaluating the loading conditions that caused the tephra to liquefy in the past, and will enable assessment of potential future hazards in the region.

For those purposes a series of undrained monotonic and cyclic triaxial tests were performed on reconstituted pumiceous samples, comprising ~52% non-plastic, pumiceous fines. The main aims of this study were to determine: (1) the monotonic behaviour; (2) the undrained

cyclic behaviour; (3) the liquefaction resistance; and (4) the extent of particle crushing after testing, of the pumiceous sandy silt. The monotonic tests were also used to develop the critical state line (CSL) of the material in order to analyse the cyclic testing results within the critical state framework. Comments on the meaning of the results from the three main objectives with regards to the paleoliquefaction features found in this tephra are given as well.

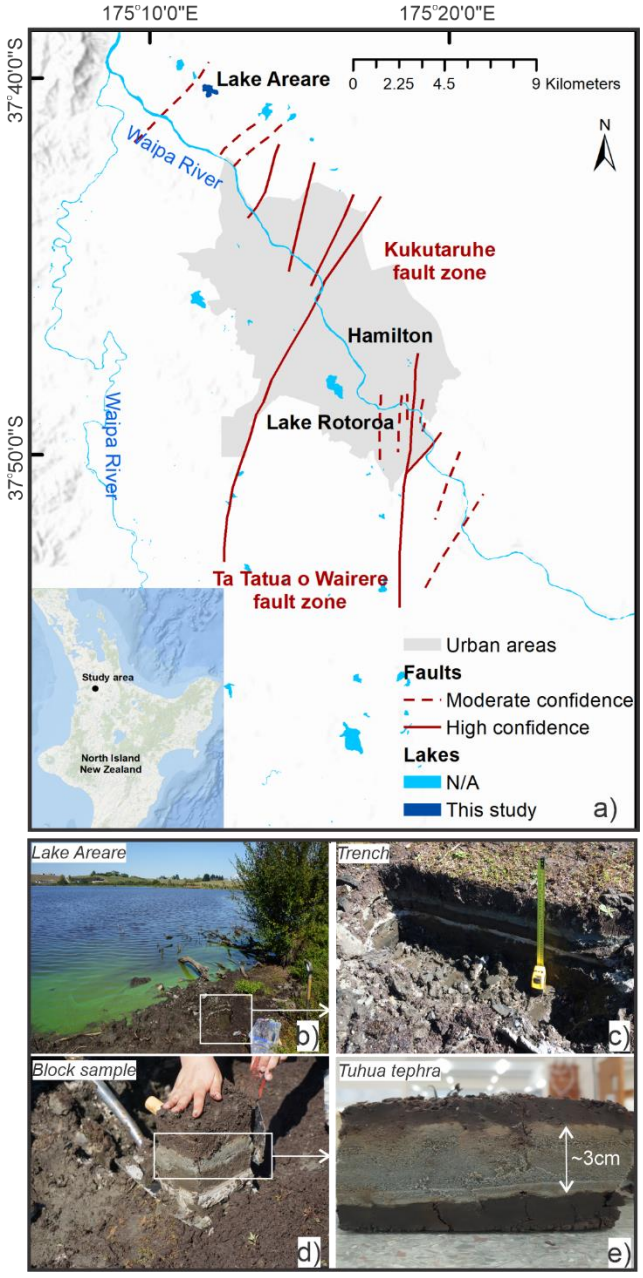

Fig. 1. Location of the sampling area for Tuhua silt (i.e., Tuhua tephra) at Lake Areare in the Hamilton lowlands and faults in the area, North Island, New Zealand. Recently identified faults are from [27,68] (a). Figure also shows (b) Lake Areare, (c) trench where the blocks were sampled, (d) block samples containing Tuhua tephra in between organic lake sediment layers, and (e) Tuhua tephra isolated from the block sample ready for contamination (organic leftovers) clean up

2. Study area

The North Island lies on the Australian Plate and is dominated by tectonic activity and active volcanism as the Pacific Plate is subducted beneath it [24,25]. Although identified as having low to medium seismic hazard, a short historical record means that an understanding of the magnitude of past earthquakes in the Hamilton lowlands area is poor [26,27]. The lowlands are within the depocentre of numerous tephra-fall deposits derived from eruptions of volcanic centres in the Taupō Volcanic Zone, Egmont/Taranaki volcano, and Tuhua Volcanic Centre (Mayor Island) during the late Quaternary, and contain a number of ~20,000-year-old riverine-peat lakes in which many tephra layers have been well-preserved with minimal post-depositional alteration [28,29] (Fig. 1a). Several of these tephra layers preserved within the sediments of the lakes have liquefied due to past earthquakes [23]. The tephra layers are pumiceous silts, sandy silts, silty sands and sands [30]. This study analysed the cyclic undrained behaviour and liquefaction resistance of the Tuhua tephra, a peralkaline rhyolitic fall-bed derived from an eruption of Mayor Island 7,600 (calendar) years ago [28,29].

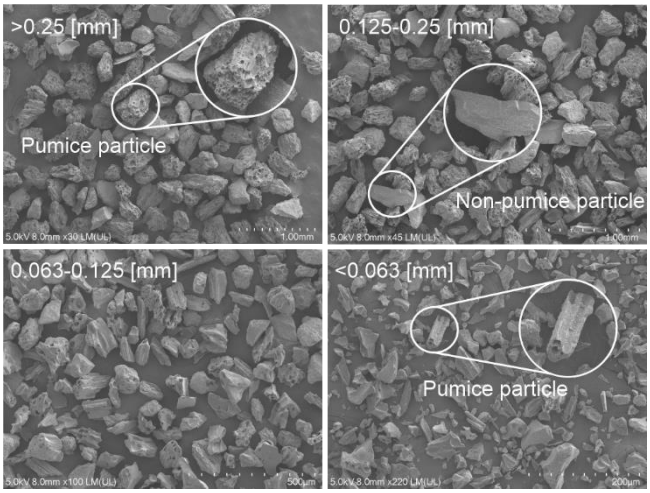

Fig. 2. SEM images of Tuhua silt separated in four grain-size fractions (< 0.063 mm, 0.063-0.125 mm, 0.125-0.25 mm and > 0.25 mm)

3. Methods and material

3.1. Sampling procedure

Sampling of Tuhua tephra was undertaken at the shore of Lake Areare (Fig. 1a and b), where the material was located at a relatively shallow sediment depth of <0.5 m in the exposed lake bed (Fig. 1c). A large number of small block samples (each with volumes of ~0.0075 m^3) were taken (Fig. 1d), which comprised the ~3 cm-thick Tuhua tephra layer and organic lake sediment above and below the tephra layer. The Tuhua tephra layer (Fig. 1e) was then carefully sampled using a spoon, cleaned from organic contamination, and oven-dried at 40°C.

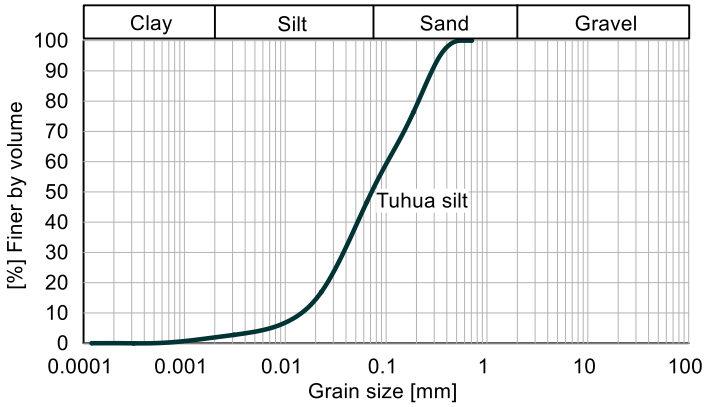

Fig. 3. Grain-size distribution of Tuhua silt prior to triaxial testing

3.2. Sample properties

A number of physical and geotechnical properties for the Tuhua tephra were obtained to accompany the triaxial testing campaign, including grain-size distribution, particle density, minimum and maximum dry densities, Atterberg limits, pumice content, and particle shape indices. The grain-size distribution of Tuhua tephra was obtained before (virgin soil) and after triaxial testing (i.e. after reconstitution, consolidation and shearing) through laser diffraction analysis using a Malvern Mastersizer 3000. The tephra soil classification and fines content threshold (%<0.075 mm) were defined following the ASTM D2487-11 [31].

The particle density was determined using a Quantachrome Ultrapyc 1000 nitrogen-filled gas pycnometer following ASTM-D5550-14 [32].

The minimum and maximum dry densities of the samples were obtained following the Japanese standard method [33] as modified by Mijic et al. [34].

Atterberg limits were obtained following ASTM-D4318-00 [35].

The pumice content was quantified in a similar manner to that of Asadi et al. [36]: a sample was separated into different grain-size fractions (i.e., <0.063 mm, 0.063-0.125 mm, 0.125-0.25 mm and >0.25 mm) by dry sieving. The mass of each fraction was determined. Then, images of clusters representing the different grain-size fractions were obtained using scanning electron microscopy (SEM) (Fig. 2). The pumice content for each fraction was then defined by means of visual inspection of the pumiceous vs non-pumiceous particles based on three SEM images per fraction, which corresponded to a total count of about 100-140 particles per fraction. The highly vesicular rough-textured particles were defined as pumiceous particles, whereas the fragments of the pumice particles that were found to lack internal voids, namely glass shards, were considered as non-pumiceous particles (Fig. 2). In the final step, the total pumice content of the sample was calculated by averaging the pumice contents of fractions defined based on the number of pumiceous particles against the total number of particles with respect to a correction factor based on their relative mass to the total mass of the sample [36].

The particle shape analysis was performed following the methodology of Kikkawa et al. [37]. The method is based on SEM images of the different fractions (i.e., <0.063 mm, 0.063-0.125 mm, 0.125-0.25 mm and >0.25 mm) of the original Tuhua tephra using 20 particles per fraction, thus 80 particles in total. The quantification of the particle shape characteristics through the roundness coefficient (R_c), aspect ratio (A_r), and angular coefficient (A_c), are defined as follows:

$$R_c = L^2/4\pi A \quad (1)$$

$$A_r = b/a \quad (2)$$

$$A_c = \left| R_c - 1 + A_r^2/(2A_r) \right| \quad (3)$$

In the above equatons, L is the perimeter of the particle, A is the surface area of the particle, and a and b are the dimensions of the particles along the minor and major axes respectively. The particle shape indices were calculated for all 80 particles, averaged by fraction and the final values were calculated with respect to the correction factor of each fraction based on the relative mass to the total mass of sample.

The grain-size distribution curve of the Tuhua tephra (i.e. virgin soil) prior to triaxial testing is shown in Fig. 3. With fines content of 51% (of which only 4% were clay sized particles) and having tested as a non-plastic sandy silt following ASTM D-2487 [38], the tested material will be referred to as Tuhua silt (ML) hereafter. The minimum and maximum void ratios are 1.06 and 2.18, respectively. The pumice content of the silt is 48%. The roundness coefficient (R_c), aspect ratio (A_r), and angular coefficient (A_c), are 1.829, 1.466 and 1.38 respectively, classifying the particles of the Tuhua silt material as ellipsoidal, elongated and highly angular [37,39]. All the material properties of the Tuhua silt are summarized in Table 1.

Table 1. Index properties of Tuhua silt

	Gs	***D_{50}***	***FC***	***PC***	***e_{min}***	***e_{max}***	***R_c***	***A_r***	***A_c***
Material		[mm]	[%]	[%]					
Tuhua silt	2.41	0.073	51.2	48	1.06	2.18	1.83	1.47	1.38

3.3. Triaxial testing

A GDS Advanced Dynamic Triaxial Testing System was used for the triaxial testing of the samples. The samples were reconstituted using the under-compaction method following the procedure of Ladd [40]. The compressive response of the tested material in the medium-high density range in the initial tests, was indicative of the redundancy in testing looser samples, as medium-high to high dense samples already captured the transition from contractive to dilative behaviour. Moreover, loose samples are known to exhibit higher degree of soil heterogeneities affecting the undrained soil response [41,42]. Therefore, the target densities

in the testing campaign were above the medium-dense range according to the relative density designations as per Terzaghi and Peck [43].

The target size of the triaxial samples was 50 mm in diameter and 100 mm in height. Deaired and demineralised water was added to the samples until a water content of 15% was obtained. Then, samples were reconstituted in eight layers into a split mould mounted on top of the triaxial base plate. For the first layers a percent undercompaction ratio of 0% was selected for reconstituting samples at high relative densities, whereas an undercompaction ratio of 15% was chosen for reconstituting samples at medium to medium-high relative densities. The definition of the undercompaction ratio is defined in the original publication of Ladd [40]. The density distribution throughout the sample was checked by observing the shape of the sample once reconstituted and its failure pattern, following the recommendations of Ladd [40].

After reconstituting the sample, the top cap was placed on the sample and the cell was assembled and filled with water. Before the saturation phase, the sample was flushed with deaired and demineralized water through the back-pressure pump. A B-value of more than 0.95 was reached once the sample was subjected to back pressures of at least 800 kPa over 15 h in the saturation stage. During the B-value check, the cell pressure was increased by 70 kPa and 20 kPa for effective consolidation pressures σ_c' corresponding to 100 kPa and 20 kPa, respectively [44]. More details about the tests and their specific conditions are summarized in Table 2. Two levels of consolidation pressure were used in this study. The effective consolidation pressure σ_c' = 20 kPa was considered to most accurately represent the stress conditions in the in-situ Tuhua silt and σ_c' = 100 kPa effective consolidation stress was used in order to compare the undrained behaviour and liquefaction resistance of the studied material with other soil types from the literature. Many other researchers have performed triaxial tests on soil materials under low confining stresses before [45–47]. However, because the consolidation pressure of 20 kPa is considered to be at the lower end of what the sensors of the triaxial apparatus are able to measure, a supplementary Fig. S1. is provided to show that the data quality of the 20 kPa consolidation pressure tests in this study. The results or a representative test (Tu-CY-21, Table 2.) by means of pore water pressure, deviator stress and axial strain development for a single cycle are presented. The oscillation variations of the sensors vary between 0%, for the last cycle in the axial strain vs. time plot (Fig. S1, (d)) to 12.5% in the pore water pressure vs. time plot (Fig. S1, (a)) of the corresponding amplitude. The oscillation variations are calculated by dividing the amplitude of the oscillation (e.g. 0.5/2 = 2.5 kPa, Fig.S1 (a)) with the amplitude in the corresponding peak of the cycle (e.g. 2 kPa, Fig.S1 (a)) and converting into percentage (2.5/2*100 =

12.5%). The sensors provided sufficiently high signal-noise ratios that do not affect the soil response analysis, thus generated meaningful results.

Table 2. Experimental programme

Test series	Type of test	Label	σ_c'	e_i	$Dr_{,i}$	e_c	$Dr_{,c}$	f	CSR	N_{CL}	ψ
			[kPa]					[Hz]			
1	M	Tu-CU-1	100	1.80	0.34	1.61	0.51	n/a	n/a	n/a	0.316
	M	Tu-CU-3	100	1.51	0.60	1.42	0.69	n/a	n/a	n/a	0.124
	M	Tu-CU-2	20	1.80	0.34	1.61	0.51	n/a	n/a	n/a	0.171
	M	Tu-CU-4	20	1.53	0.58	1.46	0.65	n/a	n/a	n/a	0.021
	M	Tu-CU-5	20	1.39	0.71	1.33	0.77	n/a	n/a	n/a	-0.114
	M	Tu-CUE-1	100	1.77	0.37	1.62	0.51	n/a	n/a	n/a	0.324
	M	Tu-CUE-2	20	1.76	0.38	1.62	0.50	n/a	n/a	n/a	0.181
2	Cy	Tu-CY-12	100	1.85	0.29	1.69	0.44	0.02	0.07	57	0.392
	Cy	Tu-CY-11	100	1.79	0.35	1.62	0.50	0.02	0.09	17	0.328
	Cy	Tu-CY-10	100	1.76	0.38	1.59	0.53	0.02	0.11	10	0.291
	Cy	Tu-CY-7	100	1.82	0.33	1.65	0.47	0.02	0.13	4	0.356
3	Cy	Tu-CY-4	100	n/a	n/a	1.45	0.65	0.02	0.11	45	0.154
	Cy	Tu-CY-5	100	1.48	0.63	1.43	0.67	0.02	0.13	35	0.134
	Cy	Tu-CY-2	100	1.45	0.65	1.38	0.72	0.02	0.15	31	0.083
	Cy	Tu-CY-6	100	1.49	0.62	1.40	0.70	0.02	0.17	12	0.104
4	Cy	Tu-CY-18	20	1.85	0.29	1.65	0.48	0.02	0.05	39	0.211
	Cy	Tu-CY-16	20	1.83	0.32	1.74	0.40	0.02	0.07	9	0.299
	Cy	Tu-CY-15	20	1.81	0.33	1.61	0.51	0.02	0.09	5	0.168
	Cy	Tu-CY-14	20	1.81	0.34	1.69	0.43	0.02	0.11	3	0.256
5	Cy	Tu-CY-19	20	1.49	0.61	1.42	0.68	0.02	0.1	50	-0.016
	Cy	Tu-CY-13	20	1.52	0.59	1.44	0.66	0.02	0.11	21	0.001
	Cy	Tu-CY-8	20	1.34	0.76	1.43	0.67	0.02	0.15	11	-0.009
6	Cy	Tu-CY-21	20	1.33	0.76	1.29	0.80	0.02	0.15	23	-0.149
	Cy	Tu-CY-22	20	1.35	0.75	1.28	0.81	0.02	0.13	88	-0.164
	Cy	Tu-CY-23	20	1.34	0.75	1.30	0.79	0.02	0.17	29	-0.139
7	Cy	Tu-CY-17	100	1.83	0.31	1.67	0.45	0.1	0.11	10	0.378
	Cy	Tu-CY-20	100	1.77	0.37	1.61	0.51	1	0.11	12	0.314

The post-consolidation void ratios of the samples were obtained following two different approaches. In the first approach, the volume change of the sample due to consolidation was measured by the back-pressure pump. In the second approach, the volume change due to consolidation was derived after completing the test following the procedure proposed by Verdugo and Ishihara [48]. The post-consolidation void ratios considered in this study were calculated by either (1) averaging the values from both approaches or (2) using the one value for the tests where results from both methods were not available (Table S1).

Seven monotonic undrained triaxial tests were performed on the reconstituted samples. Five tests were performed in compression and two tests in extension. The details about the testing conditions are presented in Table 2. A constant displacement rate of $\dot{s}$ = 0.1 mm/min was chosen following DIN EN ISO 17892-9 [44]. Shearing was performed until the axial strain reached ±10 to 15%.

A total of 18 cyclic undrained, stress-controlled triaxial tests were performed (Test series 2 to 6, Table 2). The cyclic stress amplitudes in these tests were applied with a frequency of f = 0.02 Hz. Additional two tests were performed to explore the frequency influence on the cyclic undrained response of the tested material (Test series 7, Table 2). Both tests were a replicate of Tu-CY-10 (Table 2.) by means of effective consolidation stress, relative density, and cyclic stress ratio ($CSR = q/(2\sigma_c')$, where q is deviator stress), with the only difference being the frequency (f = 0.1 Hz and f = 1 Hz). The results confirm that the response of the non-plastic silt is frequency independent (supplementary Fig. S2). The calculation of the cyclic stress ratio, double axial strain amplitude (ε_{da}), pore water pressure ratio ($r_u=u/\sigma_c'$, where u is the excess pore water pressure (EPWP) in kPa), and number of loading cycles to liquefaction (N_{CL}) followed ASTM D-5311 [49]. The initiation of cyclic liquefaction according to the ASTM D-5311 [49] is considered when either the double axial strain amplitude ε_{da} reaches 5 % or when the pore water pressure ratio, r_u reaches 0.9 [49].

4. Results

4.1. Monotonic triaxial test results

The effect of relative density, Dr, on the monotonic undrained response of Tuhua silt was analysed for the tests performed at the low effective consolidation pressure of 20 kPa (Fig. 4). The test with Dr = 0.51 (Tu-CU-2) exhibited a low peak strength with fully contractive behaviour. The response of the Dr=0.65 (Tu-CU-4), started with a similar stiffness as the Dr= 0.51 test (Tu-CU-2,) at small strains, peaked soon after at the phase transformation point [7] and then strain-softened as the stress path approached the critical state line in a contractive manner. The dense sample (Tu-CU-5, Dr = 0.77) exhibited a higher initial stiffness when compared to the other two (medium-dense) tests and was found to be purely dilative. The peak strength was found to increase with the increase in relative density.

The effect of effective consolidation pressure on the monotonic undrained response of Tuhua silt was analysed by plotting together all the tests performed (Fig. 5). As expected, the initial stiffness and peak strength increased with effective consolidation pressure (when comparing tests performed at similar relative densities). Furthermore, it was observed from Fig. 5 that Tuhua silt exhibited contractive behaviour within the range of relative densities $0.51 \leq Dr \leq 0.69$ which are considered to be within the medium-high to high density range.

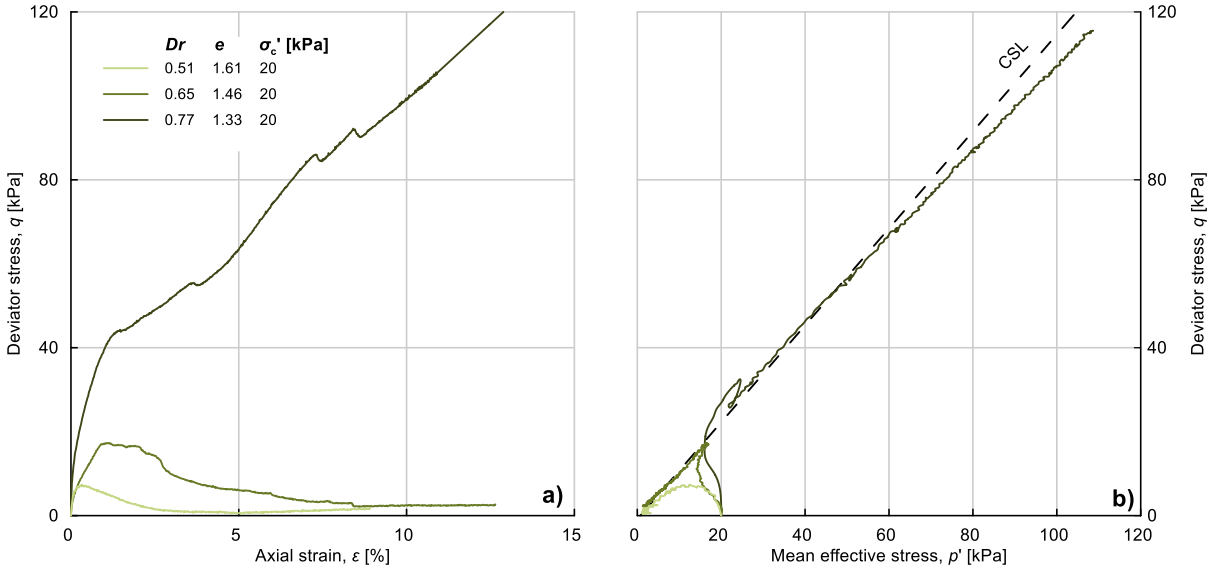

Fig. 4 Monotonic undrained compression behaviour of Tuhua silt tested at 20 kPa effective consolidation pressure. Results are presented by means of (a) stress-strain and (b) stress paths relationships

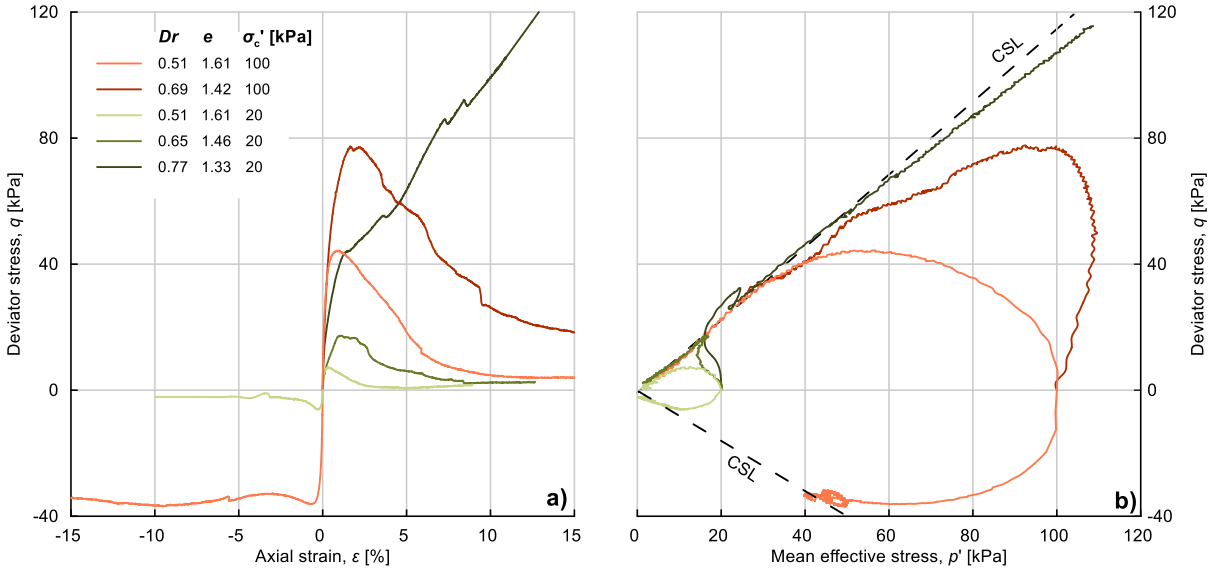

Fig. 5. Monotonic undrained behaviour of Tuhua silt tested at 20 kPa and 100 kPa effective consolidation pressure. Results are presented by means of (a) stress-strain and (b) stress paths relationships

The results from the monotonic tests were used to obtain the critical state line for the material (Fig. 6a). The start point, phase transformation point, and critical state point of individual tests as well as the critical state line are presented in Fig. 6a in the *e*-*p*' plane. The minimum and maximum void ratios obtained for Tuhua silt (i.e., at zero mean effective stress) are also plotted in the figure. It can be observed that the critical state line of Tuhua silt is located approximately in the middle between its minimum and maximum void ratios within the mean effective stress range 1 to 1000 kPa.

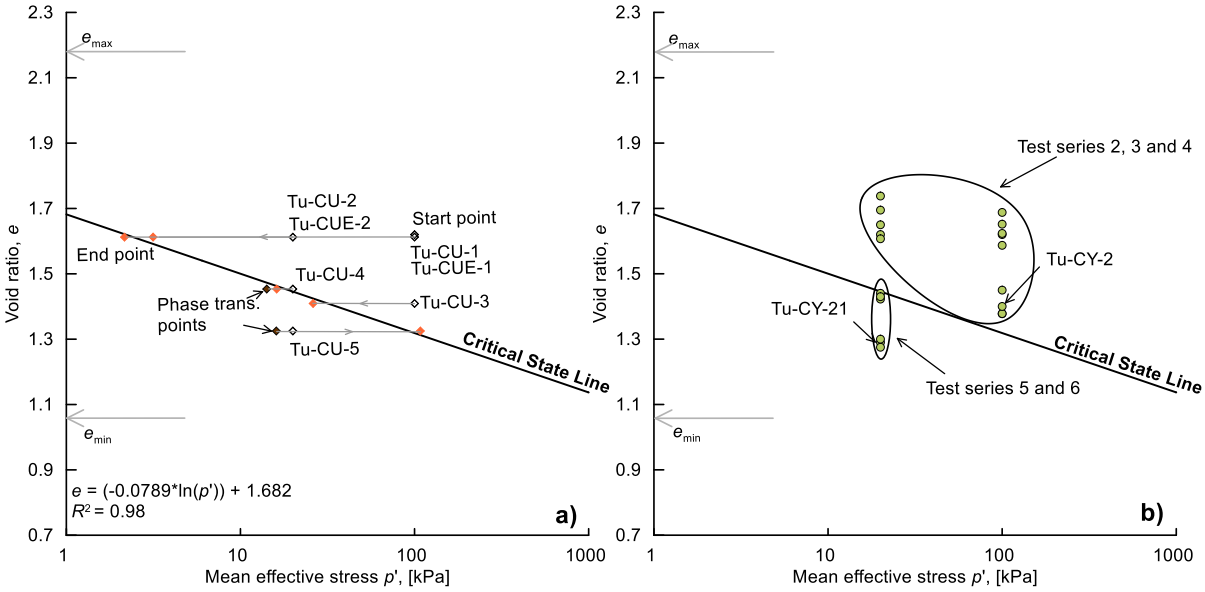

Fig. 6. (a) Critical state line (CSL) of Tuhua silt obtained from monotonic undrained triaxial tests presented together with the stress paths from monotonic compression and extension tests. White, black, and orange diamonds represent the start, phase transformation point, and critical state point, respectively. (b) Initial states (green circles) of the cyclic undrained triaxial tests presented together with the CSL of Tuhua silt

4.2. Cyclic triaxial test results

The Tuhua silt samples were found to commonly exhibit one of two types of cyclic undrained behaviour: behaviour type 1, which was characterized by a gradual increase in axial strain and EPWP in the last cycles before failure, and behaviour type 2, where a sudden response was observed with axial strain development being restricted to the last cycle prior failure. In Fig. 7, typical experimental results representing these two types of cyclic undrained behaviour are presented.

The first test (Tu-CY-21), representing cyclic undrained behaviour type 1, exhibited small axial strain for the first ~15 loading cycles, and then started to develop a gradual and steady increase in axial strain amplitude as it approached failure at 23 cycles (considering both axial strain and EPWP thresholds) (Fig. 7a). The EPWP increased in a linear manner with the loading cycles, reaching a value of around 0.95 of the initial effective consolidation pressure at failure (liquefaction). The gradual development of the liquefaction of this test under cyclic undrained testing can also be observed by considering its deviator stress-axial strain hysteresis response (Fig. 7b), where the slopes of the hysteresis loops started to gradually decrease in the last cycles.

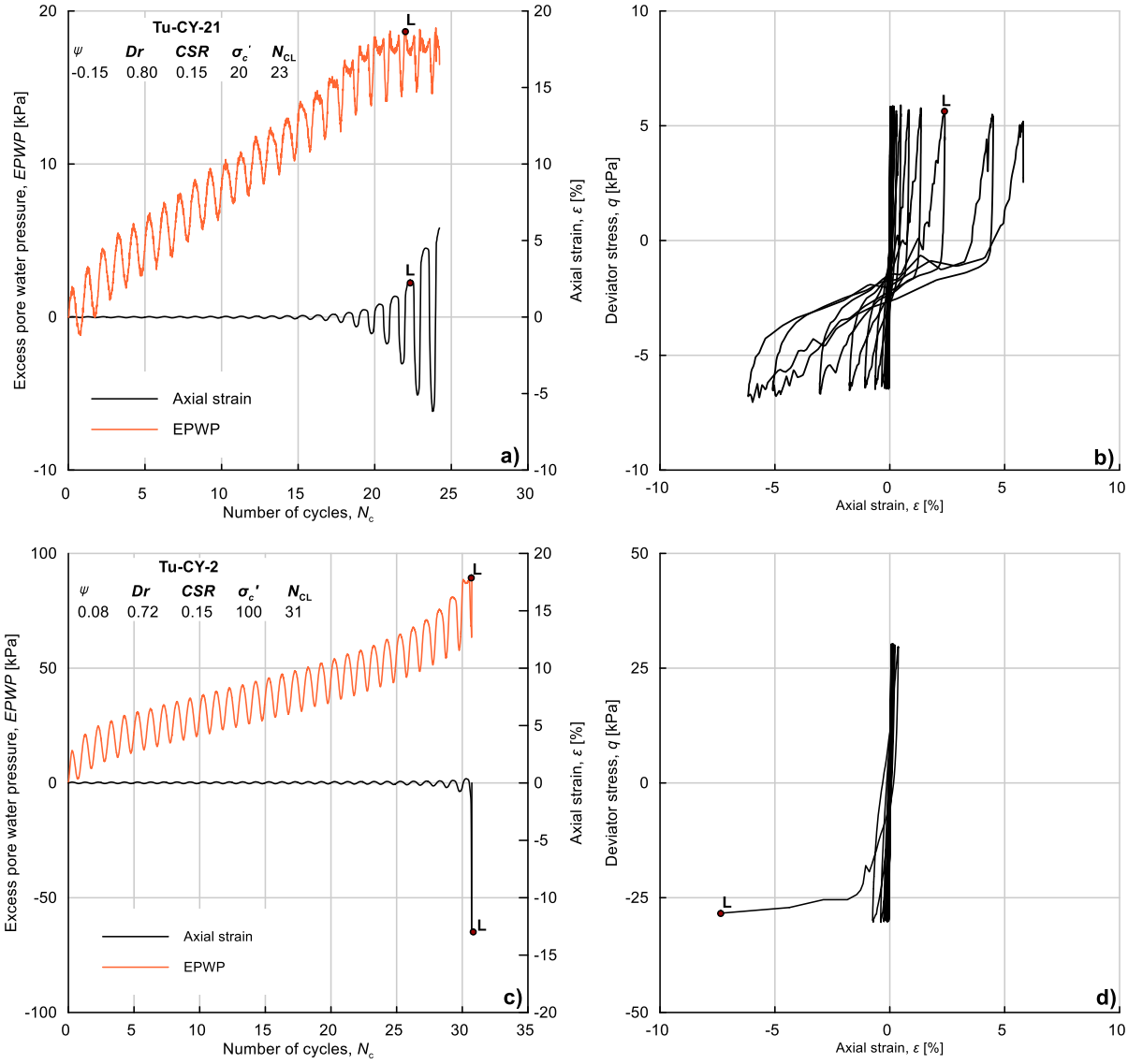

Fig. 7. Two typical examples of developments of axial strain and excess pore water pressure (left panels) and stress-strain curves (right panels). Tuhua silt samples tested in this study could be classified as exhibiting either (1) a gradual increase in axial strain and excess pore water pressure until failure – behaviour type 1 (a and b); or (2) a sudden axial strain development in the last cycle – behaviour type 2 (c and d). Note the letter "L" in the figure stands for liquefaction (initiation)

In the second example (Tu-CY-2), representing cyclic undrained behaviour type 2, the axial strain remained small for the most part of the cyclic loading, with significant axial strain developing only within the last loading cycles prior to liquefaction (Fig. 7c). Moreover, unlike the case with the behaviour type 1 tests where the accumulation of the EPWP was at a steady rate throughout the test, the EPWP in this case started off with a smaller increase in rate and then increased more rapidly during the last half of the cyclic loading until liquefaction occurred after 31 loading cycles. This test exhibited a very narrow range of

deviator stress-axial strain hysteresis loops slopes (indicating a constantly high stiffness), with the vast majority of axial strain occurring within the last loading cycle (Fig. 7d).

Both tests were performed on samples with relatively similar relative densities (i.e., *Dr* of 0.72 and 0.80). Furthermore, both samples were tested at the same cyclic stress ratio (0.15), achieved failure after a similar number of loading cycles, but were consolidated under different effective consolidation pressures. Because of the effective consolidation pressures used in the present study (i.e., 20 and 100 kPa), it is more appropriate to present the cyclic undrained results using their state parameters [50] rather than using void ratios or relative densities. The state parameter, ψ, is the difference between a given void ratio, e, and the corresponding void ratio of the steady state line, e_{ss}, for the effective consolidation stress of interest, and it incorporates the combined effect of both the void ratio and the effective consolidation stress [50]. The state parameters of all of the cyclic tests are given in Table 2. The cyclic tests are plotted against the critical state line in the *e-p'* plane in Fig. 6b.

The results by means of the development of the double amplitude axial strain, the excess pore water pressure, and the normalized number of loading cycles (N_C/N_{CL}) for all the cyclic tests performed in this study are presented in Fig. 8.

The samples tested in series 5 and 6 (i.e. with effective consolidation pressures of 20kPa and medium-dense to dense relative densities) showed negative state parameters of $-0.16 \leq \psi \leq 0.001$ (Table 2, Fig. 6b), and exhibited cyclic undrained responses that were characterized by a gradual increase in EPWP and a sudden axial strain increase at the moment of failure (i.e., cyclic undrained behaviour type 1). The remaining cyclic tests (series 2, 3, and 4), having positive state parameters of $0.08 \leq \psi \leq 0.39$, showed a more stable cyclic undrained response (i.e., cyclic undrained behaviour type 2).

Finally, the cyclic resistance ratio (CRR) data points (i.e., liquefaction resistance) for all the cyclic tests as well as their corresponding liquefaction resistance curves were obtained. In all the tests, failure occurred in a simultaneous manner, with both the double axial strain amplitude, ε_{da}, exceeding 5 % and the pore water pressure ratio, r_u , reaching 0.9 in the same loading cycle. The liquefaction resistance curves were obtained using power functions in the shape of $CSR = aN_{CL}^{-b}$, and reflect the variations in relative density, effective consolidation pressure, and state parameter (Table 2, Fig. 9). Figure 9 illustrates that the liquefaction resistance of Tuhua silt generally increased with relative density and consolidation pressure. In relation to the state parameter, higher values of the state parameter indicate lower resistance of liquefaction.

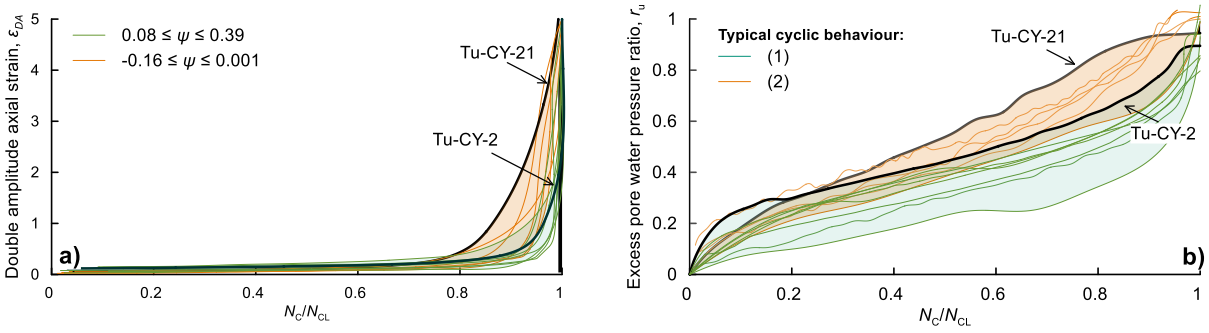

411

412 **Fig. 8.** Cyclic undrained behaviour of Tuhua silt presented by means of (a) double amplitude
413 axial strain and (b) excess pore water pressure both being plotted vs. the normalized
414 number of cycles. Green and orange shadings represent the range observed for behaviour
415 types 1 and 2 respectively. Bold lines represent the two typical examples presented in Fig 7.

416

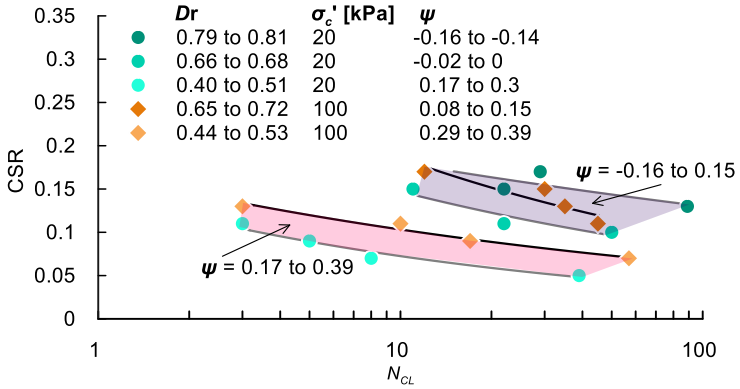

417

418 **Fig. 9.** Liquefaction resistance curves of Tuhua silt tested at three different relative densities
419 and two effective consolidation pressures, with their associated values of the state
420 parameter. Shaded areas indicate two clusters around curves which are associated with ***ψ*** =
421 -0.16 to 0.15 and ***ψ*** = 0.17 to 0.39, respectively

422 ### 4.3. Particle crushing

423 Considering the fact that the non-pumiceous particles in the Tuhua silt are defined to be the
424 pumice fragments that no longer contain internal voids, thus are considered to be less
425 crushable (although not exactly hard-grained), the potential particle crushing due to sample
426 reconstitution, consolidation, and shearing during triaxial testing was analysed by quantifying
427 the changes in grain-size parameters and pumice contents in the samples after testing. The
428 assumption here is that if particle crushing occurred, the number of pumiceous particles
429 would have decreased and the number of non-pumiceous particles (glass shards) would
430 have increased.

431 The D_{10}, D_{50}, and D_{90} grain-size parameters measured after sample reconstitution and
432 triaxial testing were plotted for all samples with respect to their built-in consolidated void
433 ratios and effective consolidation stresses (Fig. 10). By observing the mean values and their
434 standard deviations presented in Fig. 10, it is evident that (1) the effective consolidation

pressure used in this study did not significantly affect the amount of particle crushing, and (2) the pre-testing median grain size generally lies within ± 1standard deviation (SD) derived from the post-testing samples for most of the test conditions. Based on this, it can be inferred that there is no meaningful change in the grain-size distribution after testing, thus, no particle crushing occurred.

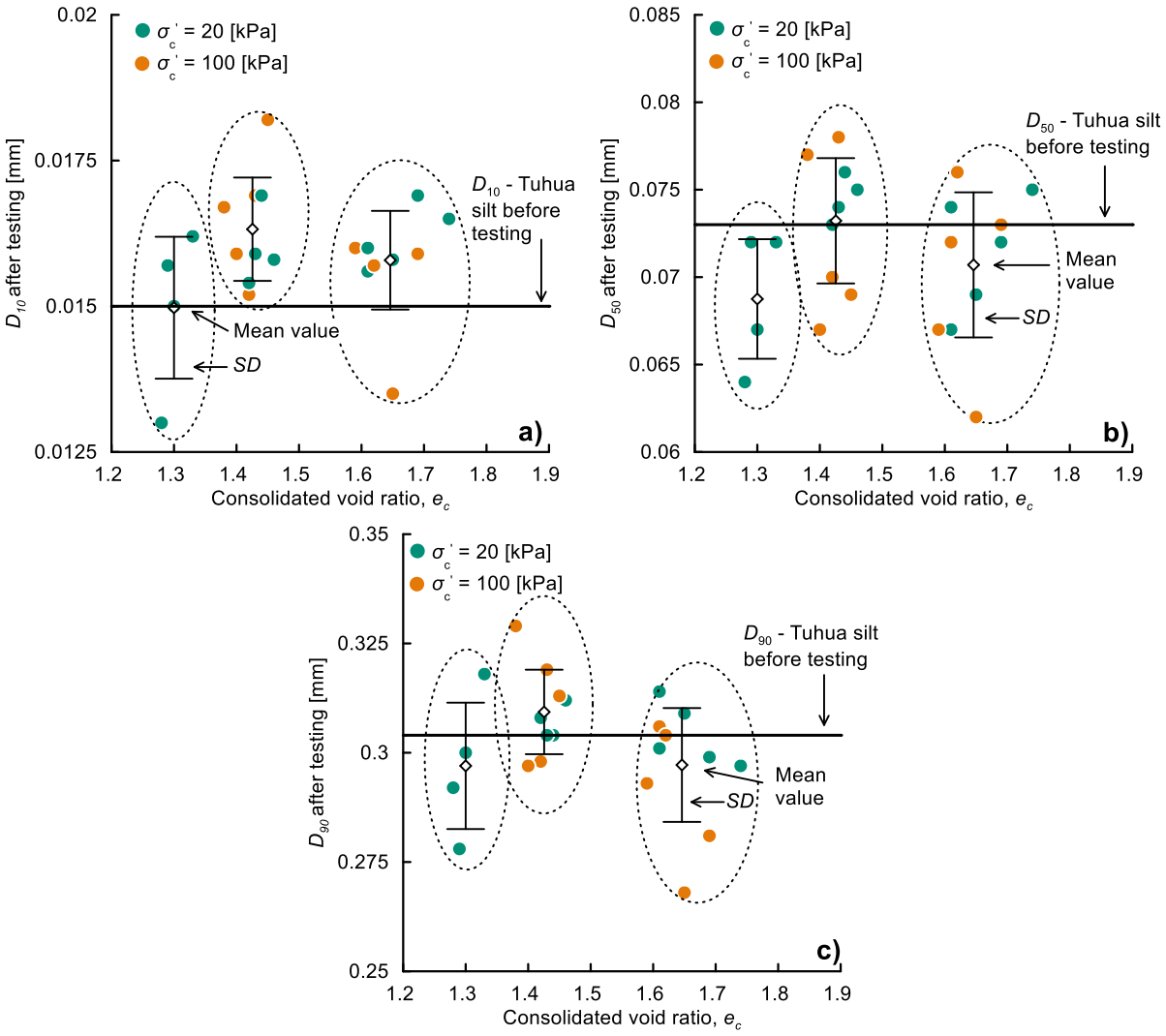

Fig. 10. Change in grain-size parameters (a) D_{10}, (b) D_{50}, and (c) D_{90} due to cyclic and monotonic triaxial tests of Tuhua silt

The second approach used SEM images of the soil particles from selected tests within a range of relative densities (1.28–1.69) for both effective consolidation pressures (20 and 100 kPa), from which the pumice contents were defined before and after testing. The hypothesis with this approach is that if the pumice content did not change, no particle crushing occurred. The five tests that were selected over a range of void ratios (relative densities) for both effective consolidation pressures are Tu-CU-5, Tu-CY-10, Tu-CY-6, Tu-CY-14 and Tu-CY-22 (Table 2). The mean pumice content per fraction for all of the selected samples is presented in Fig. 11. The mean pumice content determined before testing (grey area in Fig. 11 denotes

one SD) falls within one SD derived from the post-testing samples, suggesting no meaningful change in the pumice content, hence no particle crushing. The mean pumice contents per fraction, for the selected samples are presented in Fig. 12. These results show that the majority of the pumiceous particles are in the coarse particle range, above the fines content threshold (0.075 mm). Within the smallest fraction, the fines particles are mostly glass shards that are not particularly hard-grained but do lack the vesicularity that makes up for the lightweight and crushable characteristics of pumiceous particles.

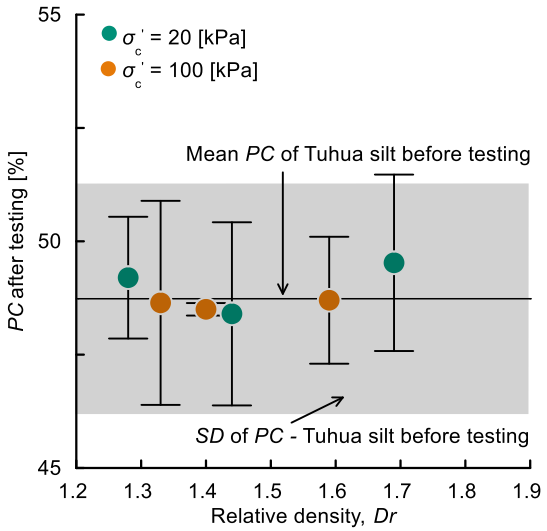

Fig. 11. Pumice contents after monotonic and cyclic triaxial testing for different relative densities

The results from both approaches that studied the potential particle crushing of the Tuhua silt indicate that no particle crushing occurred as a result of the testing and/or sample preparation method.

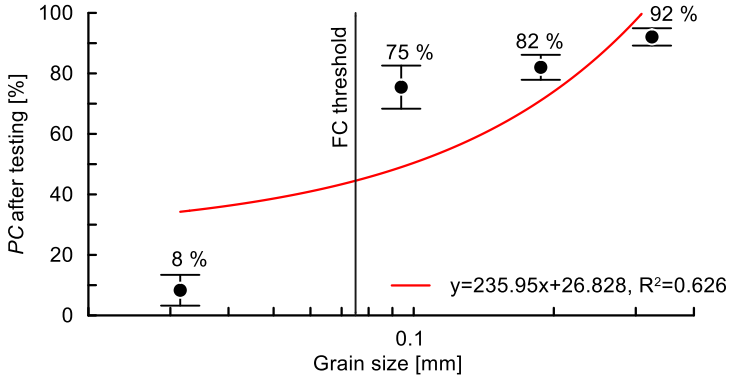

Fig. 12. Pumice contents of the four grain size fractions (< 0.063 mm, 0.063-0.125 mm, 0.125-0.25 mm and > 0.25 mm) after monotonic and cyclic triaxial testing

5. Interpretation of results and discussion

This section discusses the previously presented results by comparing the critical state line, the cyclic response, and the liquefaction resistance of Tuhua silt to these properties for other sandy and silty materials from literature, both pumiceous and hard-grained. For the interpretation, the results from the particle crushing analysis were considered as well.

5.1. Critical state line

The critical state line (or steady state line) is defined as the locus of points that describe the relationship between the void ratio and the effective confining stress in the steady state of deformation [4,51]. As a unique line that describes a particular soil, it has been used as a tool to define single physical parameters that describe sand behaviour, such as the state parameter [50] or the modified state parameter [52]. The critical state framework is well established and confirmed for hard-grained soils, yet its applicability to crushable pumiceous sands is still subject to investigation. In their study, Orense et al. [12], performed monotonic undrained tests on pure pumiceous sand samples, and found that they could not reach the steady state of deformation. They hypothesised that the breakage of particles resulted in a resistant soil structure that did not exhibit deformations at constant shear stress. De Cristofaro et al. [10], on the other hand, undertook tests on two pumiceous sands (Rangiriri and Cervinara sand). They observed contractive behaviour under a range of void ratios where they were able to obtain the corresponding critical state lines (CSL). De Cristofaro et al. compared their results with those obtained on Toyoura sand and noted differences in the positioning as well as the slopes of their critical state lines. They inferred that, as the steady-state condition represents the final state of the triaxial tests, corresponding to relatively high axial strains of ~15% where particle breakage would have occurred if the material were crushable, the CSL is a good indicator of the nature of the particles (pumiceous or not) and possible particle crushing. The hypothesised effect of the crushability of the soil material on the slope and relative positioning of the CSL was not clearly discussed by Cristofaro et al. [15]. Kramer stated that the vertical location of the CSL is influenced by gradation, whereas the slope is sensitive to the particle shape, where soils with rounded particles usually have flat CSLs [4].

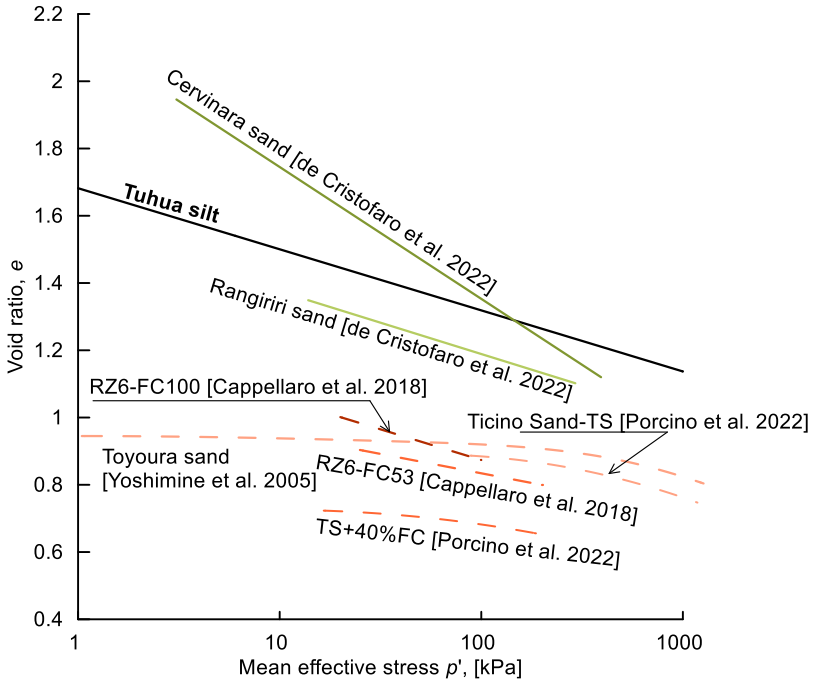

Fig. 13. Critical state lines of Tuhua silt and of representative hard-grained soils and pumiceous sands from literature

As pumiceous sandy silts have not been studied in the context of the critical state framework before, and considering the findings of Cristofaro et al. [15] and Kramer [4], an attempt to discuss the positioning and slope of the CSL of Tuhua silt against other relevant CSLs from the literature was made. The selected materials from published literature are presented in Table 3 (Materials 1 to 7).

Table 3. Geotechnical properties of selected materials from literature

	Material	Reference	Soil Classification[1]	***Gs***	***D_{50}***	***FC***	***PC***	*Testing apparatus*
					[mm]	[%]	[%]	
1	Rangiriri sand	[10]	SP	2.54	0.20	13	39	Triaxial
2	Cervinara sand	[10]	SP	2.58	0.40-0.60	10-20	n/a	Triaxial
3	Toyoura sand	[53]	SP	2.65	0.18	0	0	Triaxial
4	TS – Ticino sand	[42]	SP	2.68	0.56	0	0	Triaxial
5	TS 40% FC	[42]	SM	2.68	0.4	40	0	Triaxial
6	RZ6-FC53	[55]	ML	2.69	0.071	53	0	Direct simple shear
7	RZ6-FC100	[55]	ML	2.63	0.026	100	0	Direct simple shear
8	Pumice sand A	[12]	SP	1.95	1.15	2	~100	Triaxial
9	Pumice sand C	[12]	SM	2.38	0.07	52	~100	Triaxial
10	Shirasu Sand	[11]	SM	2.49	0.15	30	n/a	Triaxial
11	PAR	[14]	SM	2.51	0.15	30	n/a	Triaxial
12	FBM-30	[64]	SM	n/a	0.11	30	0	Triaxial

[1]Following the Unified Soil Classification System (USCS); n/a = not available

Fig. 13 shows the CSL of Tuhua silt as well as the for two natural pumiceous sands, one from New Zealand (Rangiriri sand) and the second from Italy (Cervinara sand) [15], the hard-grained representatives for sand (Toyoura and Ticino clean sands and Ticino sand with 40% fines content (FC)) [53,54] and non-plastic silts from Christchurch, New Zealand (with FC of 53% (RZ6-FC53) and 100% (RZ6-FC100)) [55]. The silt material tested in our study plots in between the CSLs of the two pumiceous sands (Rangiriri sand and Cervinara sand), and well above those of the hard-grained Toyoura and Ticino sand as well as the hard-grained silts. The gradation of soils [4] would be a relevant parameter when comparing the vertical position of the CSLs of different hard-grained soils. A more relevant parameter that would partially explain the positioning of the CSL of the pumiceous Tuhua silt in relation to the other CSLs (those of hard-grained soils included) with confidence, is the lightweight of the silt, a result of its vesicular properties. If we consider that Tuhua silt is a material that contains ~48% pumice particles, its CSL, being closely positioned to that of the pumice sands is reasonable and expected, because the void ratio range [56] of Tuhua silt is closer to the void ratio ranges of other pumiceous materials. When analysing the different slopes of the CSLs in Fig. 13, one would have to study the combined effect of particle shape and crushability [4,15]. Considering comments from both Cristofaro et al. and Kramer' [4,15], the authors hypothesised the following: particle breakage in soil particles (pumiceous or not) leads to less spherical, more angular soil particles. That would result in the original soil (with more rounded particles) having a flatter CSL than the final soil mixture (after the particle breakage). In case of a pumiceous soil, the loss of internal voids, thus lightweight properties of the vesicular particles, because of particle breakage, would also lead to a vertical offset of the CSL of the final soil mixture.

The pumiceous silt in this study was proven not crushable (Section 4.3) and therefore the slope can be discussed based on the particle shape alone. Asadi et al. [39] compared the particle shapes of Toyoura sand and a natural pumice sand from the central North Island of New Zealand, and found the pumiceous particles to be ~five times more angular than the particles of Toyoura sand particles. Considering the particle shape indices of Toyoura sand according to the Asadi et al. [39], which are R_c = 1.258, A_r = 1.483 and, Ac = 0.179 and the particle shape indices for Tuhua silt (Table 1), we conclude that the particles of Tuhua silt are ~45% more ellipsoidal, and close to eight times more angular than Toyoura sand particles. Thus, the different slopes of the CSLs of Toyoura sand and Tuhua silt, are in accordance with the findings in Kramer [4], in other words, the more angular nature of the particles of Tuhua silt compared to the particles of Toyoura sand, has resulted in a higher slope of the CSL.

5.2. Cyclic undrained response and liquefaction resistance

Whether or not cyclic liquefaction is initiated in the conventional sense ($r_u=u/\sigma_c$' reached 0.9), an analysis of the excess pore pressure as well as the axial strain development in soil during cyclic loading is of a particular interest to researchers as it provides additional insights about the loss of stiffness and strength during the loading. Clean hard-grained sands and sand-silt mixtures have received solid attention by such means in the past 50 years [57–59]. Dash and Sitharam [60] analysed the undrained excess pore pressure development of a large number of hard-grained sand-silt mixtures (Fig. 14). They tested, under a vast range of relative densities ($0.14 \leq Dr \leq 0.91$), loading frequencies ($0.1 \leq f \leq 0.5$ Hz), consolidation pressures ($50 \leq \sigma_c' \leq 200$ kPa) and critical stress ratio ($0.0922 \leq CSR \leq 0.205$). Even though they discussed trends by means of looking at a single parameter, for example, the effect of fines or relative density, they reported that all the curves generated by plotting the excess pore water pressure response against the corresponding cycle ratio fell within a relatively narrow band.

For pumiceous sands, the cyclic undrained response by means of excess pore water pressure and axial strain development until failure has provided insight for interpreting the liquefaction resistance of crushable sands compared with that of hard-grained sands [13,15]. For example, Asadi et al. [13] found that for the same relative density and effective consolidation pressure, the response of the pumiceous sand was much more stable and had a gradual failure mechanism compared with that of the hard-grained Toyoura sand, for which the onset of failure was sudden (Fig. 15.). The main reason for this difference was considered to be the subsequent particle crushing in the pumiceous sand that led to a linear increase in the double amplitude strain and a significant increase in EPWP during the first cycles. This increase was more pronounced for dense samples, whereby the samples underwent higher initial deformations and higher EPWP, indicating that the relative density played a bigger role in the undrained cyclic behaviour for pumice sands than for hard-grained sands.

The cyclic undrained response of the Tuhua silt samples consolidated under 100 kPa for two relative densities (0.44-0.53 and 0.65-0.72) was plotted and compared with the response from the hard-grained sand-silt mixtures from Dash and Sitharam's [60] study and that of the pumiceous sand and Toyoura sand used in the study by Asadi et al. [8] (Figs. 14 and 15). Note that the studies of both Dash and Sitharam and Asadi et al. were based on tests performed in a triaxial apparatus.

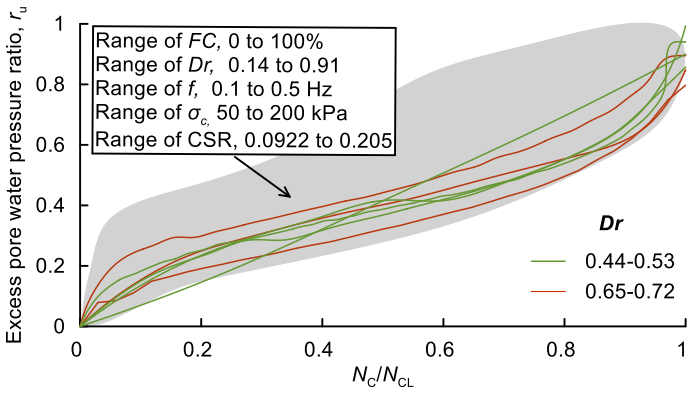

Fig. 14. Excess pore water pressure accumulation against normalized number of cycles for Tuhua silt (σ_c' = 100 kPa), plotted together with a database for the same parameters for hard-grained soil mixtures published by Dash and Sitharam [60]

By observing Fig. 14, we noticed that the results for the EPWP development during cyclic testing of Tuhua silt fall perfectly into the range established by Dash and Sitharam [46].

Fig. 15 (a) shows that for the dense pumice sand (*Dr* ≈ 0.8), the pore water pressure reached high values very quickly after loading and at small strains, and the double amplitude axial strain (Fig. 15 (b)) has a generally linear increase throughout the testing until failure. For the looser samples (*Dr* ≈ 0.3), EPWP accumulated in a steadier manner, whereas the double amplitude axial strain started increasing in the later stage of the test when the corresponding EPWP ratio r_u was around 0.5. Fig. 15 (c) and (d) show the results for Toyoura sand for two densities, where it is evident that the dense samples (*Dr* ≈ 0.8) exhibited a more gradual increase in both the pore water pressure and the axial strain, whereas the looser ones (medium-density *Dr* ≈ 0.5*)* tend to have their axial strains and EPWP develop in the last cycles of failure. By analysing Fig. 15, we observed that the effect of relative density is evident in both the pumiceous sand and the Toyoura sand, with the effect being more pronounced for the pumice sand where the differences in the undrained response are more significant. In contrast, the relative density did not seem to have a clear effect on the EPWP or axial strain development under cyclic loading of the Tuhua silt samples. However, if we consider the results for Tuhua silt presented in Fig. 8 and in Section 3.3, we observed the discussed trend based on the state parameter. In other words, samples with a negative state parameter showed a more gradual development of axial strain and EPWP compared to that of the samples with a positive state parameter.

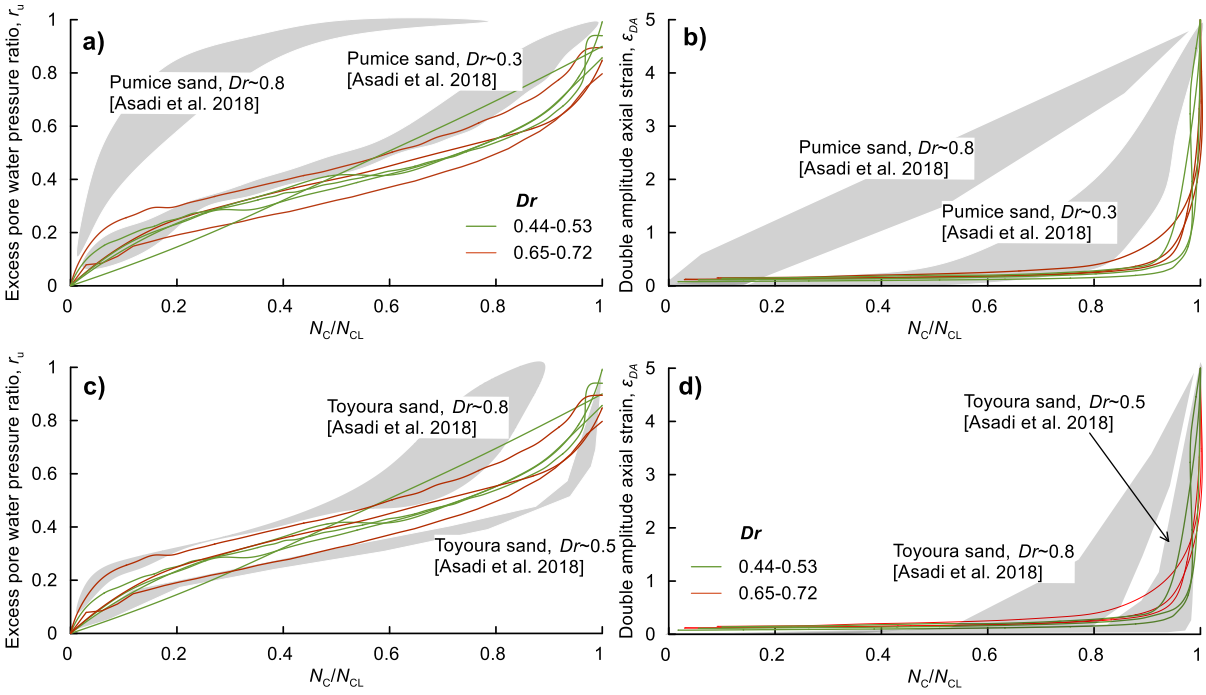

Fig. 15. (a) and (c). Excess pore water pressure ratio against normalized number of cycles for Tuhua silt against pumiceous sand and hard-grained Toyoura sand, respectively (σ_c' = 100 kPa), (b) and (d) double axial strain accumulation against normalized number of cycles for Tuhua silt against pumiceous sand and Toyoura sand, respectively (σ_c' = 100 kPa)

The liquefaction resistance is known to be dependent on relative density, effective consolidation pressure, fines content, particle shape, grain size and grain-size distribution of the material, sample reconstitution method, etc [61]. Given that the type of material tested in this study has not been tested before, we plotted its resistance against a few materials chosen from published literature. The materials used for comparison and their geotechnical properties are given in Table 3 (Materials 8 to 12).

The liquefaction resistance of the Tuhua silt for the 100 kPa consolidation stress is plotted against selected representative pumiceous and hard-grained soils from literature in Figs. 16 and 17, respectively. By analysing the curves in Fig. 16 first, we saw that the dense samples of Tuhua silt (0.65 ≤ *Dr* ≤ 0.77) show lower resistance to liquefaction than the pure pumice sand (Pumice sand A [12] *Dr* ≈ 0.7), tested at a similar relative density. The medium-dense Tuhua silt samples 0.44 ≤ *Dr* ≤ 0.53), when compared to the Shirasu sand (pumiceous sand with 30% FC, [11] *Dr* ≈ 0.5) and the PAR sand (pumiceous sand with 30%FC, [14] *Dr* ≈ 0.4), show lower resistance as well. The pumice sand with 50% FC from Orense and Pender's study [62] also shows higher liquefaction resistance in general.

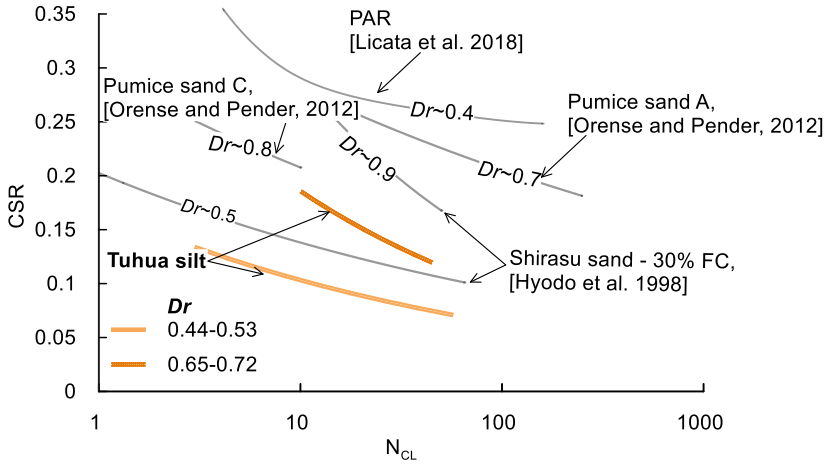

Fig. 16. Liquefaction resistance curves of Tuhua silt and relevant pumiceous soil sands (σ_c' = 100 kPa)

The Tuhua silt in this study generally shows a lower resistance when compared with hard-grained sands as well (Fig. 17). For the lower density (*Dr* = 0.44-0.53), Tuhua silt has lower resistance than Toyoura sand (*Dr* ≈ 0.5) [63], and the FBM-30 (30%FC sand, [64] *Dr* ≈ 0.5). The same is noted for the higher density (0.65 ≤ *Dr* ≤ 0.72), where Tuhua silt has lower resistance than FBM-30 (30%FC sand, [64] *Dr* ≈ 0.7). An interesting observation is made when the liquefaction resistance curves from the higher density Tuhua silt samples are compared with those for the hard-grained silt RZ6-FC53 (53%FC, [55], *Dr* ≈ 0.74): the resistance of the Tuhua silt essentially matches that of the hard-grained sandy silt from Cappellaro's study.

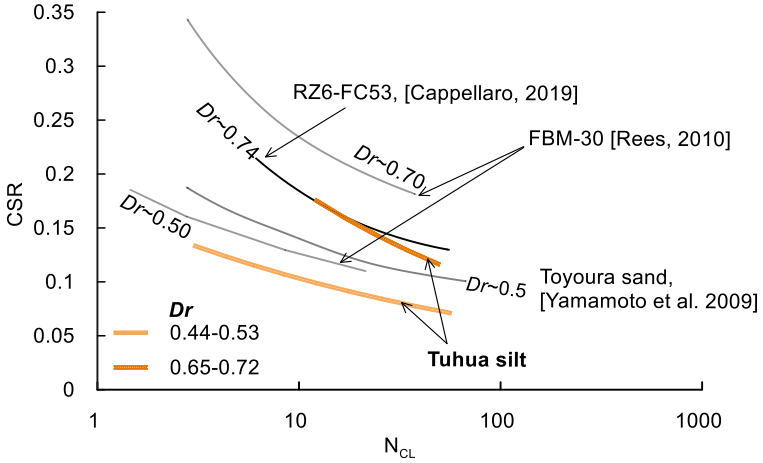

Fig. 17. Liquefaction resistance curves of Tuhua silt and relevant hard-grained sands (σ_c' = 100 kPa)

In summary the pumiceous Tuhua silt: (1) does not seem to fit into the observed trends for EPWP and axial strain development reported for pumiceous sand; (2) lies within the narrow band of a large database of hard-grained soils for the EPWP development during cyclic undrained testing; and (3) has a relatively lower liquefaction resistance than pumice and

hard-grained sands, but comes remarkably close to the resistance of the hard-grained silt with the same amount of fines.

Concise and conclusive reasoning behind the mentioned findings requires a unified testing campaign where testing uncertainties would be eliminated so that one parameter at a time could be evaluated. Acknowledging all the parameters that influence the liquefaction resistance and cyclic undrained behaviour of soils, this next section will focus on commenting on the possible influence of the pumiceous properties (i.e. pumice content and potential particle crushing) of the materials and the fines content.

Firstly, we examined the possible influence of the pumice content of the soils. Considering the fact that the pumiceous particles are prone to particle crushing and have therefore been suggested to be the main contributor to the higher liquefaction resistance of pumiceous sands [13], it is questionable why Tuhua silt (comprising a considerable amount of pumiceous particles in all grain size fractions) shows lower resistance. One explanation is that it has a moderate pumice content of 48% (compared with the ~100% pumice content in the pure pumiceous sands). In this regard, previous research on the influence of the pumice content in the liquefaction resistance of undisturbed samples found that major changes in the cyclic resistance of pumice-bearing sands were evident at relatively low proportions of pumice (i.e., 0% to 30%) in the soil mixture [65]. This finding indicates that pumice content alone might not be enough to describe the behaviour and resistance of pumiceous soil mixtures. Hence, when it comes to pumiceous properties, the next parameter to analyse was the level of particle crushing. As presented in the results section, the Tuhua silt material did not show any signs of particle crushing consequent upon sample reconstitution and triaxial testing. The fact that no particle crushing occurred in the material (within the frame of testing conditions used in the study), even with the pumice content of nearly 50%, might be the reason why Tuhua silt, in general, compares more closely with hard-grained soils than with pumiceous sands. In the context of the fines content, Hardin [66] introduced a potential for particle breakage that integrates individual fractions or grain sizes larger than 0.074 mm. He hypothesised that, the fines fraction particles are less susceptible to breakage under the same level of stresses that would cause particle crushing in coarse particles (sands and gravels), and therefore considered the potential of breakage of fines, zero. If we consider that the fines portion of Tuhua silt (particles < 0.075 mm) comprises less than 8% pumice content (Fig. 12), whereas the pumice content of the coarse particles is ~80%, we can hypothesise that the coarse particles are more susceptible to crushing than the fines. Considering the ratio of fines vs. coarse particles is almost 1:1, we assume that the fines are dominant in the soil matrix and are acting as a cushion that prevents the coarse particles from breaking during the tamping method as well as during the undrained loading from the

testing equipment (Fig. 18). In order to evaluate the threshold of fines content of the soil skeleton of the Tuhua tephra, where the role of the coarse grains becomes secondary and the fine grains govern the behaviour [67], a testing campaign that focuses on different fines contents in the Tuhua tephra is needed.

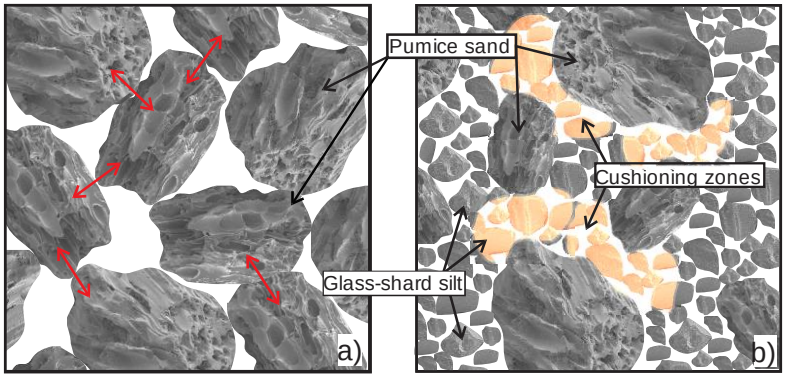

Fig. 18. Sketch of (a) pure poorly graded pumice sand and (b) sandy silt containing both pumiceous sand particles and silty glass-shard particles

Overall, the results from our study suggest that the absence of particle crushing in the Tuhua silt material during testing contributes to this material having an undrained response closer to that of hard-grained soils than to the response of pumiceous sands. These findings emphasize the possible influence of fines on the response of pumiceous soil mixtures and raise the question of whether the engineering empirical correlations (such as those based on SPT, CPT, etc.) that are considered unsuitable for pumice sands are applicable to pumice sand-silt mixtures and to what extent this applicability complicates the engineering practice when it comes to assessing the liquefaction potential of pumice soils. Furthermore, the results imply that not all pumiceous soil materials would be outside the established literature related to the development of paleoliquefaction features as well as methods for back-calculating past earthquakes based on paleoliquefaction evidence.

6. Conclusions

In this study, a natural tephra (volcanic ash) material, Tuhua silt (a distal mid-Holocene tephra layer preserved in lake sediments) with 51% fines content and 48% pumice content, sampled from the northern North Island of New Zealand, was subjected to a number of undrained triaxial tests performed at three different relative densities (medium to dense) and two different effective consolidation pressures (20 and 100 kPa). The findings from this study are summarized as follows:

- The pumiceous Tuhua silt exhibited a strain-softening response during monotonic testing even for medium-dense samples ($D_r \approx 0.65$). A strain-hardening response was observed for a relative density of $D_r \approx 0.77$. The effect of the relative density,

was in accordance with the established trends for hard-grained soils but not for those for pumiceous sands. The effect of the effective consolidation pressure is in accordance with the established trends for both hard-grained soils and pumiceous sands.

- The vertical position of the critical state line of Tuhua silt against other critical state lines from the literature was reasonable and expected when we consider the lightweight properties of the material (the void ratio range of Tuhua silt is closer to the void ratio ranges of other pumiceous materials).
  The high slope of the critical state line of Tuhua silt is a result of the high angularity of its particles.
- The cyclic undrained behaviour of Tuhua silt was dependent on the state parameter. For samples with a negative state parameter ($-0.16 \leq \psi \leq 0.001$), a more gradual development of failure was observed compared to that for samples with a positive state parameter ($0.08 \leq \psi \leq 0.39$). By means of the cyclic response, based on the observed excess pore water pressure and axial strain development, the tested material came closer to established trends more typical for those of hard-grained soils than for those of pumice sands.
- The liquefaction resistance curves of the tested material in our study were in accordance with the established trends by means of relative density i.e., higher density, resulted in higher resistance. Compared to that of both hard-grained soils and pumice sands, the liquefaction resistance of Tuhua silt is relatively low.
- Particle crushing was analysed by two methods, one that examined the change in the pumice content and the other investigated the change in the grain-size distribution of the sample before and after testing. The results from both methods indicated that no particle crushing occurred in the samples during testing.
- In general, the Tuhua silt material behaves closer to the established trends typical for hard-grained soils than to those for pumiceous sands. We infer that this conclusion is because the material did not undergo any significant particle crushing during sample reconstitution and/or testing, most probably because of a cushioning effect from the fines that prevented the coarse pumiceous particles from breaking.

Authorship contribution statement

Jordanka Chaneva: Investigation, Conceptualization, Methodology, Data curation, Writing – original draft. **Max O. Kluger:** Conceptualization, Methodology, Supervision, Writing - review and editing, Funding acquisition. **Vicki G. Moon:** Methodology, Supervision, Writing - review and editing, Funding acquisition. **David J. Lowe:** Supervision, Funding acquisition,

Writing - review and editing. **Rolando P. Orense:** Supervision, Writing - review and editing, Funding acquisition.

Acknowledgements

We acknowledge funding support from agencies of the New Zealand Government as follows: the MBIE Endeavour Fund (Smart Ideas) contract UOWX1903; the Marsden Fund contract UOW1902; the New Zealand Centre for Earthquake Resilience (QuakeCoRE); the Earthquake Commission Toka Tū Ake EQC (contract BIG 012 2020); and Waikato Regional Council (support for project on paleoseismicity and liquefaction). We thank Richard Melchert, Tehnuka Ilanko, Tom Robertson, Ben Roche, Helen Turner and Vittoria Gibbons for help in the field and/or lab, and Mrs Hekeiterangi Broadhurst (Kuia Kaumatua) and Wiremu Puke of Ngāti Wairere (Hukanui Marae), and the Department of Conservation, for supporting access to Lake Areare. Finally, we thank the anonymous referee for their constructive comments on our paper.

References

[1] Cubrinovski M, Bradley BA, Wotherspoon LM, Green RA, Bray JD, Wood C, et al. Geotechnical aspects of the 22 February 2011 Christchurch earthquake. Bull New Zeal Soc Earthq Eng 2011;44:205–26. https://doi.org/10.5459/bnzsee.44.4.205-226.

[2] Ishikawa T, Yoshimi M, Isobe K, Yokohama S. Reconnaissance report on geotechnical damage caused by 2018 Hokkaido Eastern Iburi earthquake with JMA seismic intensity 7. Soils Found 2021;61:434–41. https://doi.org/10.1016/j.sandf.2021.06.006.

[3] Ishihara K. Liquefaction and flow failure during earthquakes. Geotechnique 1993. https://doi.org/10.1680/geot.1993.43.3.351.

[4] Kramer SL. Geotechnical Earthquake Engineering. Prentice-Hall International Series in Civil Engineering and Engineering Mechanics; 1996.

[5] Robertson PK, Wride CE, List BR, Atukorala U, Biggar KW, Byrne PM, et al. The CANLEX project: Summary and conclusions. Can Geotech J 2000. https://doi.org/10.1139/t00-046.

[6] Castro G. Liquefaction and cyclic mobility of saturated sands. ASCE J Geotech Eng Div 1975;101. https://doi.org/10.1061/ajgeb6.0000173.

[7] Ishihara K, Tatsuoka F, Yasuda S. Undrained deformation and liquefaction of sand under cyclic stresses. Soils Found 1975;15:29–44. https://doi.org/10.3208/sandf1972.15.29.

[8] Seed HB, Lee KL. Liquefaction of saturated sands during cyclic loading. J Soil Mech Found Div 1966;92. https://doi.org/10.1061/jsfeaq.0000913.

[9] Youd TL, Perkins DM. Mapping liquefaction-induced ground failure potential. ASCE J Geotech Eng Div 1978.

[10] Boulanger RW, Idriss IM. Liquefaction susceptibility criteria for silts and clays. J Geotech Geoenvironmental Eng 2006;132:1413–26. https://doi.org/10.1061/(ASCE)1090-

776 0241(2006)132:11(1413).

777 [11] Hyodo M, Hyde AFL, Aramaki N. Liquefaction of crushable soils. Geotechnique 1998;48:527–
778 43. https://doi.org/10.1680/geot.1998.48.4.527.

779 [12] Orense RP, Pender MJ, O'Sullivan a S. Liquefaction Characteristics of Pumice Sands. EQC Proj
780 10/589 2012.

781 [13] Asadi MS, Asadi MB, Orense RP, Pender MJ. Undrained cyclic behavior of reconstituted
782 natural pumiceous sands. J Geotech Geoenvironmental Eng 2018;144:434–41.
783 https://doi.org/10.1061/(ASCE)GT.1943-5606.0001912.

784 [14] Licata V, D'Onofrio A, Silvestri F. Microstructural factors affecting the static and the cyclic
785 resistance of a pyroclastic silty sand. Geotechnique 2018:434–41.
786 https://doi.org/10.1680/jgeot.16.P.319.

787 [15] de Cristofaro M, Olivares L, Orense RP, Asadi MS, Netti N. Liquefaction of volcanic soils:
788 undrained behavior under monotonic and cyclic loading. J Geotech Geoenvironmental Eng
789 2022;148:04021176-(1-11). https://doi.org/10.1061/(asce)gt.1943-5606.0002715.

790 [16] Pender MJ, Robertson TW, Gilion D, Jennings N, Pemberton G. Edgecumbe earthquake:
791 Reconaissance report. Bull New Zeal Soc Earthq Eng 1987;20:201–49.

792 [17] Orense R, Vargas-Monge W, Cepeda J. Geotechnical aspects of the January 13, 2001 El
793 Salvador earthquake. Soils Found 2002;42:57–68. https://doi.org/10.3208/sandf.42.4_57.

794 [18] Kokusho T. Earthquake-induced flow liquefaction in fines-containing sands under initial shear
795 stress by lab tests and its implication in case histories. Soil Dyn Earthq Eng 2020;130:105948-
796 (1-18). https://doi.org/10.1016/j.soildyn.2019.105984.

797 [19] Bommer JJ, Rodríguez CE. Earthquake-induced landslides in Central America. Eng Geol
798 2002;63:189–220. https://doi.org/10.1016/S0013-7952(01)00081-3.

799 [20] White JDL, Houghton BF. Primary volcaniclastic rocks. Geology 2006;34:677–80.
800 https://doi.org/10.1130/G22346.1.

801 [21] Hyodo T, Wu Y, Hyodo M. Influence of fines on the monotonic and cyclic shear behaviour of
802 volcanic soil "Shirasu." Eng Geol 2022;301:106591-(1-18).
803 https://doi.org/10.1016/j.enggeo.2022.106591.

804 [22] Lowe DJ. Tephrochronology and its application: a review. Quat Geochronol 2011;6:107–53.
805 https://doi.org/10.1016/j.quageo.2010.08.003.

806 [23] Kluger MO, Lowe DJ, Moon VG, Chaneva J, Johnston R, Villamor P, et al. Seismically-induced
807 down-sagging structures in tephra layers (tephra-seismites) preserved in lakes since 17.5 cal
808 ka, Hamilton lowlands, New Zealand. Sediment Geol 2023:1–22.
809 https://doi.org/https://doi.org/10.1016/j.sedgeo.2022.106327.

810 [24] Nicol A, Seebeck H, Wallace L. Quaternary tectonics of New Zealand. Shulmeister J, Ed Landsc
811 Quat Environ Chang New Zealand Atl Adv Quat Sci 2017;3:1–34. https://doi.org/10.2991/978-
812 94-6239-237-3_1.

813 [25] Shane P. The southern end of the pacific ring of fire: Quaternary volcanism in New Zealand.
814 Landsc Quat Environ Chang New Zealand Atl Adv Quat Sci 2017;3:35–66.
815 https://doi.org/10.2991/978-94-6239-237-3_2.

816 [26] Downs G. Earthquakes. Edbrooke SW Geol Waikato Area Inst Geol Nucl Sci 1250,000 Geol
817 Map 4 Low Hutt, GNS Sci 2005:56–8.

[27] Van Dissen R, Seebeck R, N L, Barnes N, Nicols P. Development of the New Zealand community fault model – version 1.0. Proc. 2021 New Zeal. Soc. Earthq. Eng. Annu. Tech. Conf. Christchurch, 2021, p. 1–9.

[28] Lowe DJ. Controls on the rates of weathering and clay mineral genesis in airfall tephras: a review and New Zealand case study. Rates Chem Weather Rocks Miner Acad Press Orlando 1986:265–329.

[29] Lowe DJ. Stratigraphy, age, composition, and correlation of late Quaternary tephras interbedded with organic sediments in waikato lakes, North Island, New Zealand. New Zeal J Geol Geophys 1988;31:125–65. https://doi.org/10.1080/00288306.1988.10417765.

[30] Chaneva J, Kluger MO, Moon VG, Lowe DJ, Orense RP. Geotechnical properties of liquefied pumiceous layers in lakes. Proc. 7th Int. Young Geotech. Eng. Conf. – Scott © 2022 Aust. Geomech. Soc. Sydney Aust. ISBN 978-0-9946261-5-8, 2022, p. 313–8.

[31] International A. ASTM D2487-11 Standard Practice for Classification of Soils for Engineering Purposes (Unified Soil Classification System). ASTM Stand Pract (ASTM Int 2011.

[32] ASTM-D5550-14. Standard test methods for specific gravity of soil solids by water pycnometer. Am Soc Test Mater 2014.

[33] Japanese Geotechnical Society Standard J-2009. Test method for minimum and maximum densities of sand 2009.

[34] Mijic Z, Bray JD, Riemer MF, Cubrinovski M, Rees SD. Test method for minimum and maximum densities of small quantities of soil. Soils Found 2021;61:533–40. https://doi.org/10.1016/j.sandf.2020.12.003.

[35] ASTM-D4318-17e1. Standard test methods for liquid limit, plastic limit and Plasticity index of Soils. Am Soc Test Mater 2017.

[36] Asadi MS, Orense RP, Asadi MB, Pender MJ. Maximum dry density test to quantify pumice in natural soils. Soils Found 2019;59:532–43. https://doi.org/10.1016/j.sandf.2019.01.002.

[37] Kikkawa N, Orense RP, Pender MJ. Observations on microstructure of pumice particles using computed tomography. Can Geotech J 2013. https://doi.org/10.1139/cgj-2012-0365.

[38] ASTM-D-2487. Classification of soils for engineering purposes (USCS). Am Soc Test Mater 2018.

[39] Asadi MB, Asadi MS, Orense RP, Pender MJ. Dynamic behaviour of undrained natural pumiceous soils. Proc. 20th NZGS Geotech. Synposium, 2017.

[40] Ladd RS. Preparing test specimens using undercompaction. Geotech Test J 1978;1:16–23.

[41] Hariprasad C, Rajashekhar M, Umashankar B. Preparation of uniform sand specimens using stationary pluviation and vibratory methods. Geotech Geol Eng 2016. https://doi.org/10.1007/s10706-016-0064-0.

[42] Kluger MO, Kreiter S, Stähler FT, Goodarzi M, Stanski T, Mörz T. Cone penetration tests in dry and saturated Ticino sand. Bull Eng Geol Environ 2021. https://doi.org/10.1007/s10064-021-02156-y.

[43] Terzaghi K, Peck RB. Soil mechanics in engineering practice. Second edi. Wiley International, New York, 1967; 1967.

[44] V. DI für N e. DIN EN ISO 17982-8, 2018. Geotech Investig Test - Lab Test Soil - Part 8

Unconsolidated Undrained Triaxial Test (ISO 17892-82018); Ger Version EN ISO 17892-82018 n.d.

[45] Fannin RJ, Eliadorani A, Wilkinson JMT. Shear strength of cohesionless soils at low stress. Geotechnique 2005. https://doi.org/10.1680/geot.2005.55.6.467.

[46] Lancelot L, Shahrour I, Al Mahmoud M. Failure and dilatancy properties of sand at relatively low stresses. J Eng Mech 2006. https://doi.org/10.1061/(asce)0733-9399(2006)132:12(1396).

[47] Huang Y, Cheng HL, Osada T, Hosoya A, Zhang F. Mechanical behavior of clean sand at low confining pressure: verification with element and model tests. J Geotech Geoenvironmental Eng 2015. https://doi.org/10.1061/(asce)gt.1943-5606.0001330.

[48] Verdugo R, Ishihara K. The Steady State of Sandy Soils. Soils Found 1996;36:81–91. https://doi.org/10.3208/sandf.36.2_81.

[49] ASTM D 5311 - 92. Standard test method for load controlled cyclic triaxial strehgth of soil. Am Soc Test Mater 2004. https://doi.org/10.1520/D5311-11.2.

[50] Been K, Jefferies MG. A state parameter for sands. Geotechnique 1985;35:99–112. https://doi.org/10.1680/geot.1985.35.2.99.

[51] Castro G. Liquefaction of sands. Harvard Univ, Harvard Soil Mech Ser 81 1969.

[52] Bobei DC, Lo SR, Wanatowski D, Gnanendran CT, Rahman MM. Modified state parameter for characterizing static liquefaction of sand with fines. Can Geotech J 2009;46:281–95. https://doi.org/10.1139/T08-122.

[53] Yoshimine M, Nishizaki H, Amano K, Hosono Y. Flow deformation of liquefied sand under constant shear load and its application to analysis of flow slide of infinite slope. Soil Dyn Earthq Eng 2006;26:253–64. https://doi.org/10.1016/j.soildyn.2005.02.016.

[54] Porcino DD, Triantafyllidis T, Wichtmann T, Tomasello G. Using different state parameters for characterizing undrained static and cyclic behavior of sand with non-plastic fines. Soil Dyn Earthq Eng 2022;159:107318-(1-17). https://doi.org/10.1016/j.soildyn.2022.107318.

[55] Cappellaro C, Cubrinovski M, Bray JD, Chiaro G, Riemer MF, Stringer ME. Liquefaction resistance of Christchurch sandy soils from direct simple shear tests. Soil Dyn Earthq Eng 2021;141:106489-(1-14). https://doi.org/10.1016/j.soildyn.2020.106489.

[56] Cubrinovski M, Ishihara K. Maximum and minimum void ratio characteristics of sands. Soils Found 2002;142:65–78. https://doi.org/10.3208/sandf.42.6_65.

[57] Dobry R, Ladd RS, Yokel FY, Chung RM, Powell D. Prediction of pore water pressure buildup and liquefaction of sands during earthquakes by the cyclic strain method. Natl Bur Stand Build Sci Ser 1982.

[58] Wang JN, Kavazanjian E. Pore pressure development during non-uniform cyclic loading. Soils Found 1989. https://doi.org/10.3208/sandf1972.29.2_1.

[59] Hazirbaba K, Rathje EM. Pore pressure generation of silty sands due to induced cyclic shear strains. J Geotech Geoenvironmental Eng 2009;135. https://doi.org/10.1061/(asce)gt.1943-5606.0000147.

[60] Dash HK, Sitharam TG. Undrained cyclic pore pressure response of sand-silt mixtures: Effect of nonplastic fines and other parameters. Geotech Geol Eng 2009;27:501–17. https://doi.org/10.1007/s10706-009-9252-5.

[61] Ishihara K. Soil behaviour in earthquake geotechnics. 1997. https://doi.org/10.5860/choice.34-5113.

[62] Orense RP, Pender MJ, O'Sullivan a S. Liquefaction characteristics of pumice sands. EQC Proj 2012.

[63] Yamamoto Y, Hyodo M, Orense RP. Liquefaction resistance of sandy soils under partially drained condition. J Geotech Geoenvironmental Eng 2009. https://doi.org/10.1061/(asce)gt.1943-5606.0000051.

[64] Rees SD. Effects of fines on the undrained behaviour of Christchurch sandy soils. University of Canterbury, 2010.

[65] Stringer M. Response of pumice-rich soils to cyclic loading, 2022, p. 1–15.

[66] Hardin BO. Crushing of soil particles. J Geotech Eng 1985;111:1177–92. https://doi.org/10.1061/(ASCE)0733-9410(1985)111:10(1177).

[67] Thevanayagam S, Shenthan T, Mohan S, Liang J. Undrained fragility of clean sands, silty sands, and sandy silts. J Geotech Geoenvironmental Eng 2002. https://doi.org/10.1061/(asce)1090-0241(2002)128:10(849).

[68] Moon V, Lange WD. Potential shallow seismic sources in the Hamilton Basin: final report for EQC project No 16/717 2017.

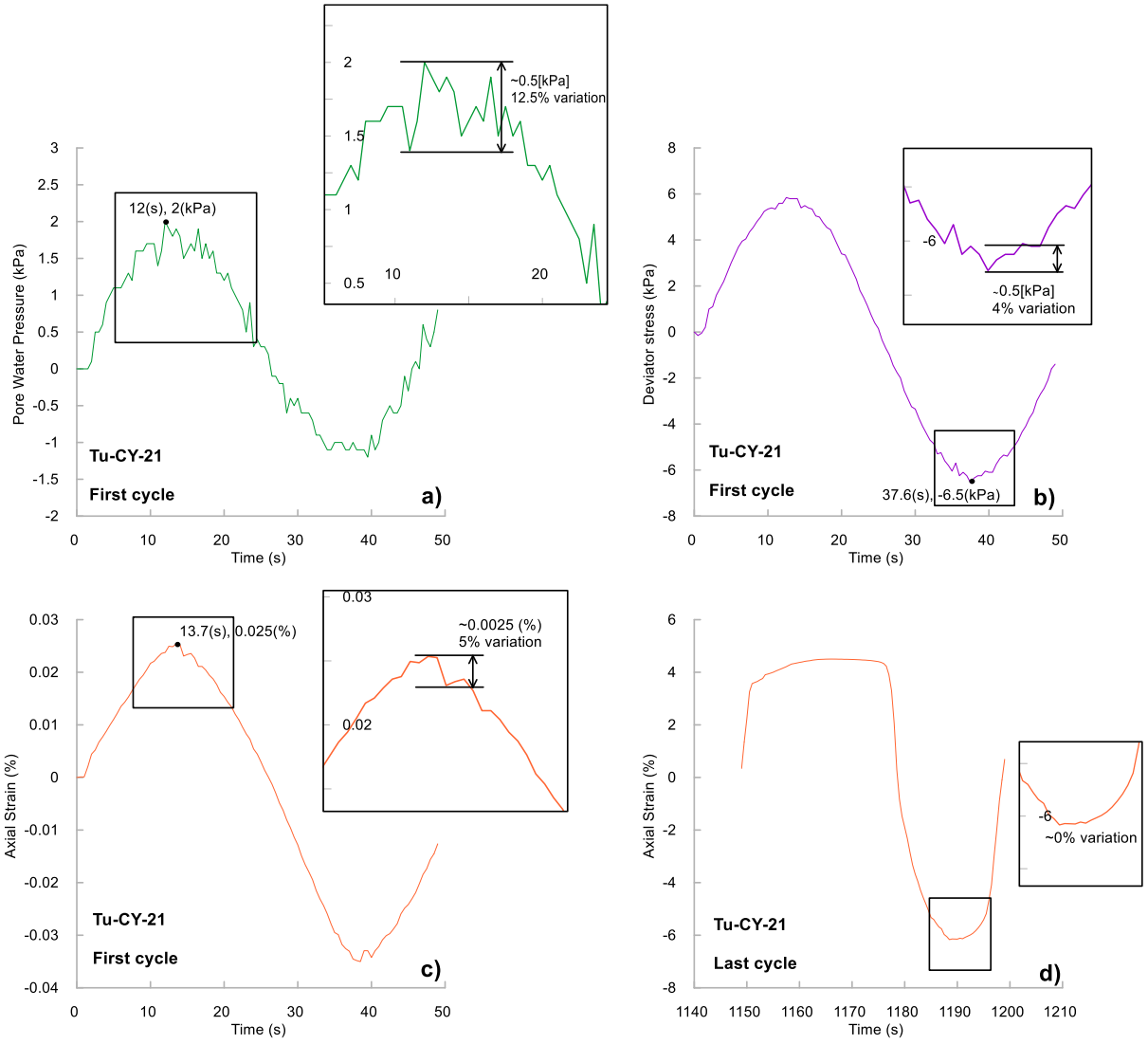

Fig. S1. Pore water pressure (a), deviator stress (b) and axial strain (c) and (d) vs time plots for a single cycle (first or last) of test Tu-CY-21, showing the transducer oscillations in order to confirm the data quality of the tests

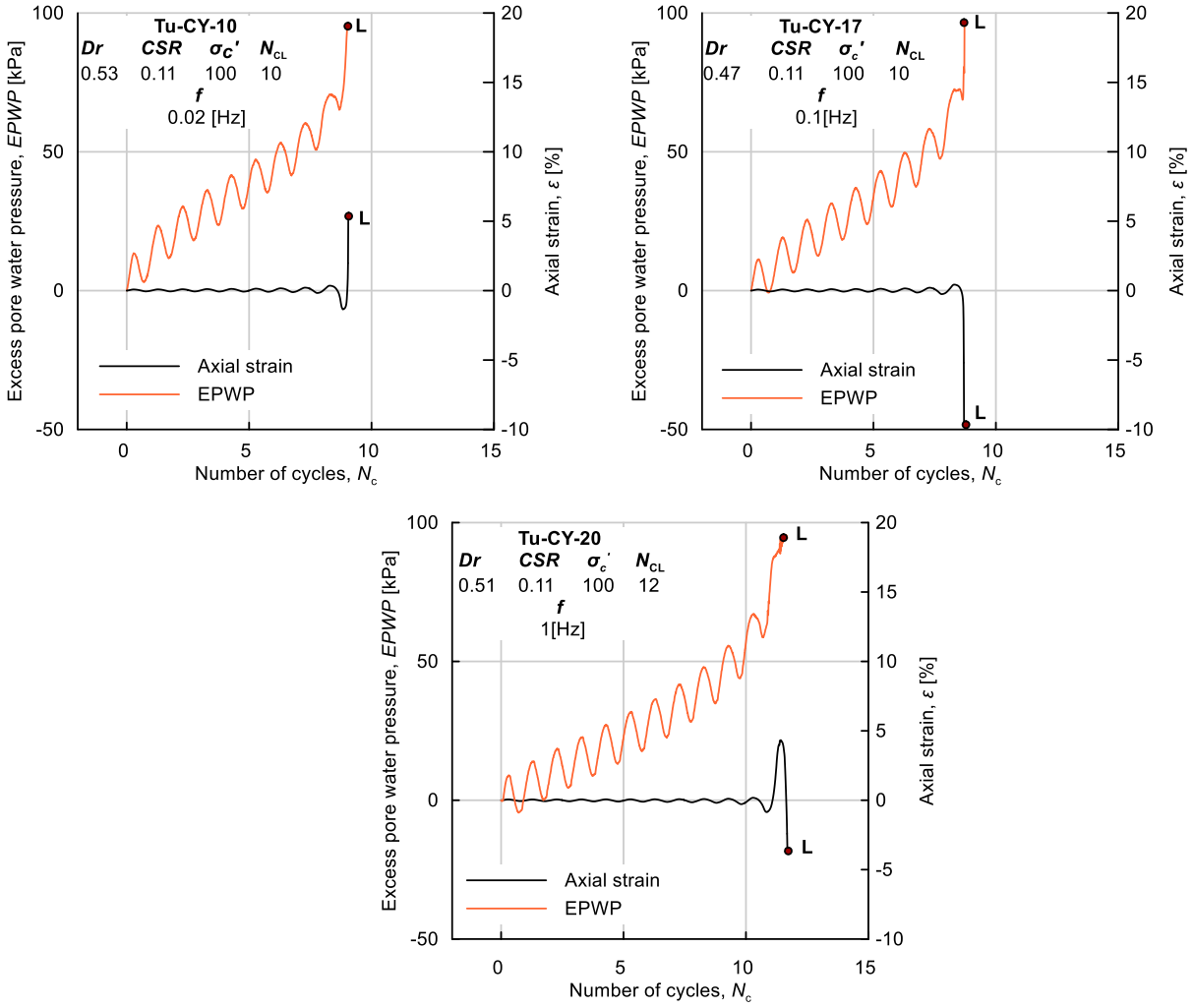

Fig. S2. Developments of axial strain and excess pore water pressure for tests Tu-CY-10, Tu-CY-17 and Tu-CY-20 that were tested under the similar conditions by means of relative density, (***Dr*** ≈ 0.5), effective consolidation stress ($\boldsymbol{\sigma_c}'$ = 100kPa) and same cyclic stress ratio (*CSR* = 0.11) with a different loading frequency (***f*** = 0.02, 0.1 and 1 Hz respectively)

938 Table S1. Void ratio and relative density, initial as well as consolidated values, from both
939 method (1) based on sample dimensions before testing and sample volume loss during
940 consolidation and method (2) based on the Verdugo and Ishihara [48] procedure

Test series	Type of test	Label	e_i	$Dr_{,i}$	e_{c1}	e_{c2}	$Dr_{,c1}$	$Dr_{,c2}$	e_c	$Dr_{,c}$
1	Monotonic	Tu-CU-1	1.80	0.34	1.61	0.51	n/a	n/a	1.61	0.51
	Monotonic	Tu-CU-3	1.51	0.60	1.41	0.69	1.42	0.68	1.42	0.69
	Monotonic	Tu-CU-2	1.80	0.34	1.61	0.51	n/a	n/a	1.61	0.51
	Monotonic	Tu-CU-4	1.53	0.58	1.45	0.65	1.46	0.64	1.46	0.65
	Monotonic	Tu-CU-5	1.39	0.71	1.31	0.78	1.34	0.75	1.33	0.77
	Monotonic	Tu-CUE-1	1.77	0.37	1.62	0.50	n/a	n/a	1.62	0.51
	Monotonic	Tu-CUE-2	1.76	0.38	1.62	0.51	1.62	0.50	1.62	0.50
2	Cyclic	Tu-CY-12	1.85	0.29	1.69	0.44	n/a	n/a	1.69	0.44
	Cyclic	Tu-CY-11	1.79	0.35	1.62	0.50	n/a	n/a	1.62	0.5
	Cyclic	Tu-CY-10	1.76	0.38	1.59	0.53	n/a	n/a	1.59	0.53
	Cyclic	Tu-CY-7	1.82	0.33	1.65	0.47	n/a	n/a	1.65	0.47
3	Cyclic	Tu-CY-4	/	/	n/a	n/a	1.45	0.65	1.45	0.65
	Cyclic	Tu-CY-5	1.48	0.63	1.38	0.72	1.49	0.62	1.43	0.67
	Cyclic	Tu-CY-2	1.45	0.65	1.38	0.72	n/a	n/a	1.38	0.72
	Cyclic	Tu-CY-6	1.49	0.62	1.39	0.71	1.40	0.70	1.40	0.7
4	Cyclic	Tu-CY-18	1.85	0.29	1.76	0.37	1.53	0.58	1.65	0.48
	Cyclic	Tu-CY-16	1.83	0.32	1.74	0.40	n/a	n/a	1.74	0.4
	Cyclic	Tu-CY-15	1.81	0.33	1.61	0.51	n/a	n/a	1.61	0.51
	Cyclic	Tu-CY-14	1.81	0.34	1.69	0.43	n/a	n/a	1.69	0.43
5	Cyclic	Tu-CY-19	1.49	0.61	1.42	0.68	n/a	n/a	1.42	0.68
	Cyclic	Tu-CY-13	1.52	0.59	1.44	0.66	1.44	0.67	1.44	0.66
	Cyclic	Tu-CY-8	1.34	0.76	1.45	0.65	1.42	0.68	1.43	0.67
6	Cyclic	Tu-CY-21	1.33	0.76	1.27	0.82	1.31	0.78	1.29	0.8
	Cyclic	Tu-CY-22	1.35	0.75	1.28	0.81	n/a	n/a	1.28	0.81
	Cyclic	Tu-CY-23	1.34	0.75	1.30	0.79	1.29	0.74	1.30	0.79
F	Cyclic	Tu-CY-17	1.83	0.31	1.67	0.45	n/a	n/a	1.67	0.45
	Cyclic	Tu-CY-20	1.77	0.37	1.61	0.51	n/a	n/a	1.61	0.51

941 n/a = not available
942